Visual Neuroscience (1998), **15**, 1157–1174. Printed in the USA.

A phenomenological model of visually evoked spike trains in cat geniculate nonlagged X-cells

NICOLAS GAZÈRES, LYLE J. BORG-GRAHAM, AND YVES FRÉGNAC

Equipe Cogniscience, Institut Alfred Fessard, CNRS, Avenue de la Terrasse, 91198 Gif-sur-Yvette, France

(RECEIVED March 6, 1998; ACCEPTED June 9, 1998)

Abstract

The visual information that first-order cortical cells receive is contained in the visually evoked spike trains of geniculate relay cells. To address functional issues such as the ON/OFF structure of visual cortical receptive fields with modelling studies, a geniculate cell model is needed where the spatial and temporal characteristics of the visual response are described quantitatively. We propose a model simulating the spike trains produced by cat geniculate nonlagged X-cells, based on a review of the electrophysiological literature. The level of description chosen is phenomenological, fitting the dynamics and amplitude of phasic and tonic responses, center/surround antagonism, surround excitatory responses, and the statistical properties of both spontaneous and visually evoked spike trains. The model, which has been constrained so as to reproduce the responses to centered light spots of expanding size and optimal light and dark annuli, predicts responses to thin and large bars flashed in various positions of the receptive field. The switching gamma renewal process method has been introduced for modelling spontaneous and visually evoked spike trains within the same mathematical framework. The statistical structure of the spike process is assumed to be more regular during phasic than tonic visual responses. On the whole, this model generates more realistic geniculate input to cortex than the currently used retinal models.

Keywords: Cat, Lateral geniculate nucleus, Phenomenological model, Center/surround antagonism, Spike train, Renewal process

Introduction

The cat lateral geniculate nucleus (LGN) is characterized by a remarkably low level of convergence between the different functional streams originating in the retina. Anatomical (Hamos et al., 1987; Robson, 1993) and physiological studies (Singer & Creutzfeldt, 1970; Cleland et al., 1971; Coenen & Vendrik, 1972; Kaplan & Shapley, 1984; Cleland & Lee, 1985; Mastronarde, 1992) support the view that the retino-geniculate projection is so specific that one relay cell receives its retinal input from very few (1–3) ganglion cells, at least within the X pathway. In various respects, geniculate receptive fields (RFs) are very similar to those of retinal ganglion cells. For example, they exhibit an antagonistic center/surround organization (Hubel & Wiesel, 1961), have roughly the same average center size at a given excentricity (Cleland et al., 1971; Mastronarde, 1992), and can be classified into very similar physiological X,Y, or W classes (Hoffmann et al., 1972; Wilson et al., 1976).

The main elaborations that occur in the RF of LGN relay cells with respect to the RF of retinal afferents are due, among other things, to the influence exerted by inhibition (Singer & Creutzfeldt, 1970; Sillito & Kemp, 1983) and consist of lower levels of spontaneous and evoked activity (Cleland & Lee, 1985), enhanced center/surround antagonism (CSA; Maffei & Fiorentini, 1972; Hammond, 1973), sharper separation between phasic and tonic discharges (Bullier & Norton, 1979), different statistics in the maintained spike discharge (Bishop et al., 1964), and a contribution of burst firing to the response (Guido et al., 1992; Mukherjee & Kaplan, 1995).

Recent models of cat visual cortex have taken advantage of the similarities between retina and LGN by modelling the geniculate input to the cortical network as a direct transfer of the retinal signal (Wehmeier et al., 1989; Wörgötter & Koch, 1991; Somers et al., 1995). Taking a retinal model as direct input to a cortical model is justified because these cortical models have addressed the issue of orientation selectivity, namely, a feature not present in the LGN and considered to emerge only at the cortical level (but see Vidyasagar & Urbas, 1982). The retinal models (Linsenmeier et al., 1982; Richter & Ullman, 1982) have simply been used to provide the cortical network with light-modulated synaptic excitation.

When addressing issues like the ON/OFF organization and subfield antagonism of cortical simple cells, it is necessary to have the right degree of CSA in the geniculate input. Since CSA is less pronounced in the retina than in the geniculate, using a retinal model as direct input to first-order cortical cells would drive them too strongly in response to large stimuli. Sharpening the existing retinal CSA level by modelling intrageniculate inhibitory inter-

Correspondence and reprint requests to: Yves Frégnac, Equipe Cogniscience, Institut Alfred Fessard, CNRS, Avenue de la Terrasse, 91198 Gif-sur-Yvette, France.

actions explicitly would be very expensive in the perspective of large-scale neural simulations. Therefore, we preferred to keep the simplicity and efficiency of the phenomenological retinal models while extending their structure and updating the parameters closer to the known properties of geniculate relay cells.

Because visually evoked spike trains are intrinsically stochastic, a spike train model should take intertrial variability into account in addition to the average response. While the statistics of *spontaneous* geniculate activity has been extensively studied in the literature (e.g. Teich et al., 1997), no model of the *visually evoked* discharge has emerged yet. We have reviewed the experimental evidence available to date on geniculate firing during visual stimulation and we conclude that a simple point-process model is sufficient as a first approximation.

In this paper, we propose and discuss a phenomenological model of individual nonlagged X geniculate RFs, built from a review of the electrophysiological literature in the cat. This work has four original features: (1) we focus on the restricted case of flashed bars and radial symmetry of the spatial filters, which permits simple analytical equations to be derived; (2) free parameters are introduced that allow for separate tuning of the amplitude and dynamics of the phasic and tonic discharges; (3) the degree of CSA and the amplitude of the excitatory responses evoked from RF surrounds have been set to match their physiological level in the LGN; and (4) geniculate spike trains have been generated by a new and simple method, the switching gamma renewal process, which allows to model phasic and tonic responses with different statistics. This model has been used as a realistic front-end in a modelling study of the ON/OFF organization of visual cortical RFs (Gazères et al., 1997).

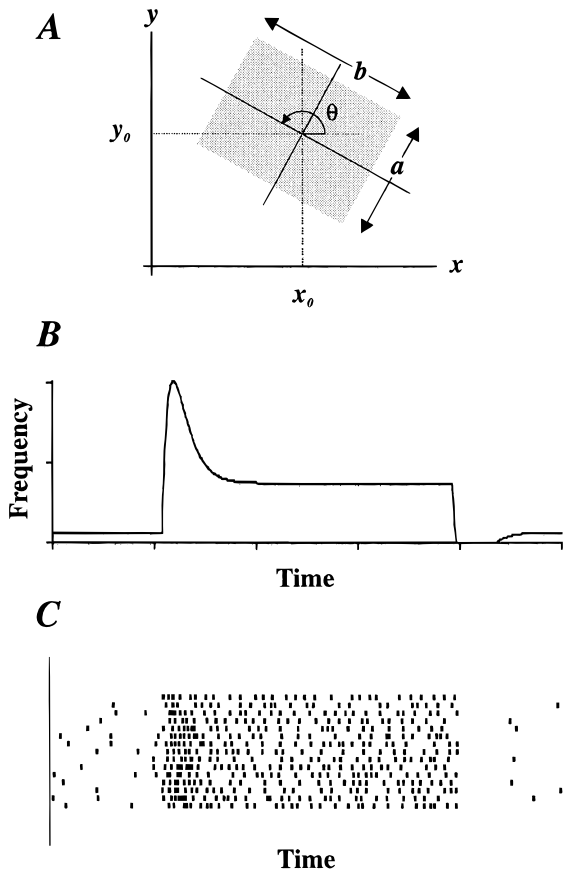

Fig. 1. Model overview. A: A stimulus is first specified in the visual plane (x, y). The origin represents the center of the model geniculate RF. Here, a rectangular bar is centered at (x_0, y_0), of width a and length b. The length axis of the bar makes the angle θ with the x axis. B: A number of spatiotemporal filters (see text and Fig. 2) is then used to convert the stimulus specification (A) into a continuous frequency waveform. C: Spike trains are generated from the frequency waveform (B) using a switching GRP. Visual examination shows that each raster bears strong similarity to the frequency waveform and yet exhibits some degree of intertrial variability. All rasters are aligned on time of stimulus presentation.

Methods

Overview

Our purpose here is to develop a model that generates the signal that first-order cells in cortex receive, namely, spike trains statistically comparable to the discharge of individual geniculate cells in response to visual excitation. While model spike trains should exhibit some degree of intertrial variability, the histograms constructed by accumulating n realizations of such spike trains should converge to the usual visual poststimulus time histograms (PSTHs), as $n \to \infty$. The model proceeds in two steps: first, the stimulus specification (Fig. 1A) is converted into a frequency waveform (Fig. 1B) which is the theoretical counterpart of the PSTH; second, spike trains are generated by a stochastic point process whose rate function $f(t)$ is the previously obtained frequency waveform (Fig. 1C).

Stimulus specification

A spot is specified by its center location (x_0, y_0) and diameter D. A bar is specified by its center location, width a and length b and angle θ between the abscissa and the major axis ($0 \leq \theta < \pi$). Stimulus contrast is modelled with a single scalar I (equivalent to $\log \Delta L/L$, where L is the luminance). Contrast is not systematically varied in this article, so in most cases, a bar brighter than the background has contrast $I = +1$ and a bar darker than the background has contrast $I = -1$. Conventionally, an ON transition refers to the appearance of a stimulus; an OFF transition refers to the stimulus extinction. For instance, the ON transition of a dark bar is a decrease in luminance. Stimuli are presented at time t_0 and removed at time t_1, so the time-variable stimulus contrast $I(t)$ can be described by the following piecewise constant function:

$$I(t) = I_0, \quad \text{if } t_0 \leq t < t_1, \qquad I(t) = 0 \text{ otherwise} \tag{1}$$

Model structure for ON-center nonlagged X-cells

The model computes the contributions of eight sets of parallel filters (Figs. 2 and 3). Each set is composed of a spatial integration stage, followed by a convolution in the time domain and a nonlinearity. The contributions of the eight sets are then summed together with a constant level of background activity. The result is passed through a half-wave rectification, yielding the final waveform. Parameter values are summarized in Fig. 2 and an example is shown in Fig. 3.

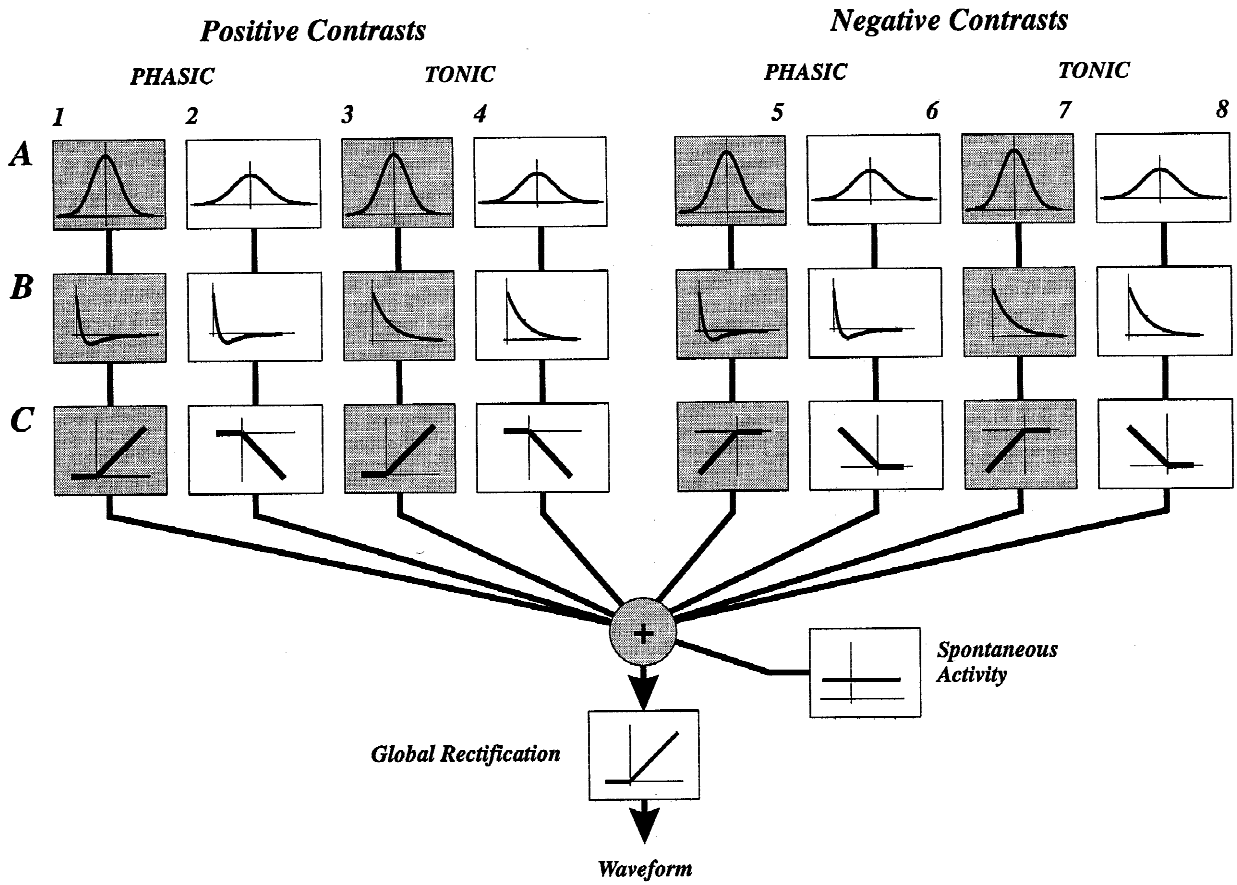

Fig. 2. Spatiotemporal filters for the ON-center cell model. Spatiotemporal filters are numbered from 1 to 8, and consist of a spatial (A), a temporal (B), and a nonlinear (C) stage (see Methods). The result of passing the stimulus through each of the eight sets of filters A, B, C yields a function of time. These eight contributions are summed along with a constant level of spontaneous activity, and the result is passed through a global rectification, producing the final frequency waveform. Columns with grey boxes represent center contributions (see narrower Gaussians, row A); columns with white boxes represent surround contributions (wider Gaussians). Columns 3–4 and 7–8 in row B build the tonic component of the response; columns 1–2 and 5–6 in row B generate the phasic component. Spatial parameters: A1, A3, A5, A7, $\sigma = 0.11$ deg. A2, A4, A6, A8, $\sigma = 0.33$ deg. Temporal parameters: B1, B2, B5, B6, $\tau_1 = 13$ ms, $\tau_2 = 15$ ms. B3, B4, B7, B8, $\tau = 15$ ms. B1, B2, $A = 3370$. B3, B4, $B = 74$. B5, B6, $A = 1900$. B7, B8, $B = 33$. Nonlinearities: C1, C3, $\Psi(x)$. C2, C4, $-\Psi(x)$. C5, C7, $-\Psi(-x)$. C6, C8, $\Psi(-x)$ (see Methods).

Spatial filters

An individual LGN cell receives excitatory input from only a few retinal ganglion cells. This excitatory input can be visually evoked from a narrow retinal region overlapping the geniculate RF center. A geniculate cell also receives visually driven inhibitory input, the exact shape of which is not agreed upon (see Discussion) but the extent of which is known to be wider than the excitatory input. Following the methods introduced for retinal models (Rodieck, 1965; Linsenmeier et al., 1982; Richter & Ullman, 1982), the spatial dependence of such excitatory and inhibitory contributions to a receptive field has been described here by circular bidimensional Gaussians:

$$G(x,y) = \frac{1}{2\pi\sigma^2}\exp\left(-\frac{x^2+y^2}{2\sigma^2}\right).$$

The Gaussian width is determined by the space constant σ. For all σ, the volume $\iint G(x,y)\,dx\,dy$ under the surface equals 1. In Fig. 2, row A, boxes with odd numbers (narrow Gaussians) represent the spatial dependence of the center mechanism, while boxes with even numbers (wide Gaussians) represent the spatial dependence of the surround mechanism. The operation carried out at this first stage is simply the spatial product between the stimulus and the Gaussian profile (see Appendix).

Temporal filters

The impulse response stage is implemented to specify the temporal dynamics of the waveform. In Fig. 2, impulse responses in boxes B1–B2, and B5–B6 specify the phasic component of the discharge and impulse responses in boxes B3–B4, and B7–B8 the tonic one. Impulse responses in B1–B2 and B5–B6 are high-pass filters, modelled as a difference of exponentials:

$$h_{phasic}(t) = A\left[\frac{1}{\tau_1}\exp\left(\frac{-t}{\tau_1}\right) - \frac{1}{\tau_2}\exp\left(\frac{-t}{\tau_2}\right)\right], \quad t \geq 0. \qquad (2)$$

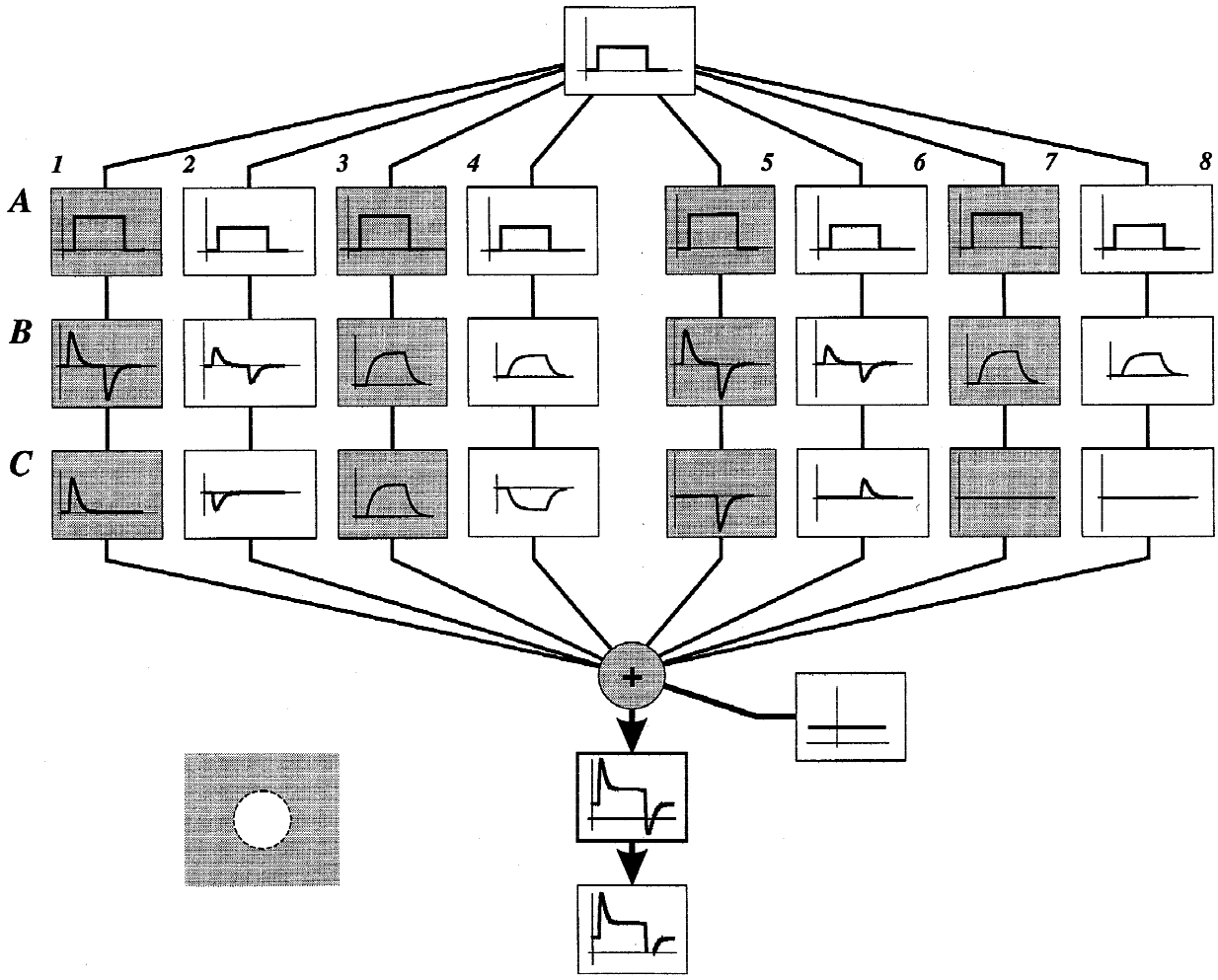

Fig. 3. Example of a frequency waveform computation. Inset at lower left shows an example stimulus: an optimal centered spot (white disk) flashed on a grey background. Each box contains the result of the sequence of signal transformations laid out in Fig. 2. Top box shows the temporal specification of the stimulus contrast $I(t)$ [eqn. (1)]. Boxes in row A plot the result $p(t)$ of the spatial integration stage; these are simply scaled versions of $I(t)$ [eqn. (A3)]. Boxes in row B plot the result of the convolution in the time domain. B1–B2 and B5–B6 contain the phasic templates $W_{phasic}(t)$ resulting from applying the high-pass impulse response $h_{phasic}(t)$; B3–B4 and B7–B8 contain the tonic templates $W_{tonic}(t)$ resulting from applying the exponential impulse response $h_{tonic}(t)$. Row C holds the result of passing each box in row B through the associated nonlinearity. The eight contributions are then added together, along with the spontaneous activity level. Note that the OFF transition results in a "negative frequency" at that stage (thick box). Lastly, the global rectification eliminates all possible negative discharge, yielding the final frequency waveform (see text).

Impulse responses in B3–B4 and B7–B8 are low-pass filters implemented as exponentials:

$$h_{tonic}(t) = \frac{B}{\tau} \exp\left(\frac{-t}{\tau}\right), \quad t \geq 0. \tag{3}$$

In Fig. 2, the phasic and tonic impulse responses have been split and represented separately for the sake of clarity. In addition, separating temporal filters into phasic and tonic components makes the fit of phasic and tonic response amplitudes simpler. The phasic and tonic temporal waveforms for a step of contrast are obtained by convolving the time-dependent output of the spatial stage [eqn. (12)] with $h_{phasic}(t)$ and $h_{tonic}(t)$, respectively:

$$W(t) = \int_{-\infty}^{\infty} p(u)h(t-u)\,\mathrm{d}u.$$

The inhibitory signal is likely to be of longer latency than the excitatory retinal input, since at least part of it is of intrageniculate origin. However, we did not model this delay explicitly because intracellular recordings have shown that inhibitory postsynaptic potentials (IPSPs) can sometimes be recorded slightly ahead of excitation (Singer et al., 1972), suggesting that the delay has some intrinsic variability and is not critically needed to get plausible geniculate responses.

Nonlinear stage

The nonlinear stage (Fig. 2, row C) uses the following half-wave rectification function: $\Psi(x) = x$, when $x > 0$, and $\Psi(x) = 0$, when $x \leq 0$. The nonlinearity of each given set of filters has two characteristics. First, the position of the zero branch about the origin determines whether the contribution comes from an ON- or OFF-

center retinal afferent and which contrast change it allows to get through. Second, the positive or negative value of the nonzero branch determines whether the corresponding afferent input acts through direct excitation or polysynaptic inhibition onto the postsynaptic geniculate cell.

For example, C1 and C3 represent the excitatory influence elicited by positive contrast change in the RF center. C2 and C4 represent the inhibitory influence exerted by positive contrast changes in the surround. C5 and C7 represent the inhibition evoked by negative contrast changes in the center. C6 and C8 represent the excitation evoked by negative contrast changes in the surround. The left half of Fig. 2 is called the "positive contrast" side because nonlinearities retain only positive contrast changes. The right half deals with negative contrast changes. As stated earlier, C1–C2 and C5–C6 operate on the phasic response while C3–C4 and C7–C8 transform the tonic response.

Center/surround antagonism is implemented at the nonlinearity stage. Consider each of the nonlinearity pairs C1–C2, C3–C4, C5–C6, and C7–C8. In a given pair, the first nonlinearity is associated with a center contribution, and the second one with a surround contribution having the same phasic/tonic property. The nonlinearities in the pair retain the same contrast change, but introduce a sign reversal between the center and the surround contributions, which means that the center and the surround contributions will act antagonistically.

An example of frequency waveform derivation

Fig. 3 shows how the model works in the case of a light spot flashed in an ON-center RF. The excitatory contribution from the ON-center mechanism is stronger than the inhibition from the OFF-surround. The product of the stimulus with the spatial filters returns a higher value for the center Gaussians (row A, grey boxes) than for the surround Gaussians (row A, white boxes). The impulse response stage (row B) then transforms the piecewise constant functions of row A into phasic and tonic templates with an appropriate time course. The nonlinearity stage (row C) operates on the templates by eliminating either the positive or the negative parts of the phasic responses. For example, C1–C4 only retain the positive part of the curves above them in row B, which correspond to the positive contrast change. In addition, C2 and C4 change the sign of the curve, so that, in the following summation the *surround* contribution of filter 2 will antagonize the *center* contribution of filter 1; this implements center/surround antagonism for the phasic response. Likewise, C4 antagonizes C3 for the tonic response to ON transitions of light stimuli.

Box C6 (Fig. 3) shows that the OFF transition of the centered spot evokes a weak excitation from the OFF-surround, strongly antagonized by the ON-center inhibitory influence (box C5), the net result being a suppression. Boxes C7–C8 illustrate that in the model the extinction of the visual stimulus produces no tonic component; in this case, the OFF transition just evokes a suppressive transient. If the stimulus instead was a light annulus flashed in the OFF-surround, then the value of the spatial integration would be higher for the surround than for the center, and the frequency waveform would be negative, consistent with the suppression classically observed in this case (Fig. 8B).

Gamma renewal processes

The second step in simulating visually evoked geniculate spike trains is to generate a spike train whose rate follows the frequency waveform $f(t)$. There is experimental evidence that the statistical properties of spontaneous activity and tonic visual responses are different from those of phasic visual responses (see Discussion). In particular, initial phasic responses are more regular than in a Poisson process, which could be caused by an increased contribution of bursts. Underestimating this regularity could introduce too much variability in the *number* of geniculate spikes present in the phasic discharge, thereby disorganizing the visual input onto first-order cortical cells. Therefore, the switching gamma renewal process method was applied, which allows to merge portions of spike trains with different regularity levels.

Constant-rate gamma renewal processes

Renewal processes are processes in which the interevent intervals are independent and identically distributed random variables (Cox, 1962). These processes have already been used to model neural spike trains in retina and LGN (Kuffler et al., 1957; Bishop et al., 1964; e.g. Teich et al., 1997). A constant-rate gamma renewal process (GRP) is a renewal process where intervals are realizations of a random variable T following a *gamma* probability density function (*pdf*), with parameter $\lambda > 0$ and regularity $r > 0$:

$$g_T(t) = P\{t < T < t + \mathrm{d}t\} = \lambda \frac{(\lambda t)^{r-1}}{\Gamma(r)} \exp(-\lambda t), \quad t \geq 0, \tag{4}$$

where $\Gamma(r)$ is defined as $\Gamma(r) = \int_0^\infty t^{r-1} \exp(-t)\mathrm{d}t$. Such a process has a mean rate $f = \lambda/r$. Intervals have a mean duration $\mu_T = r/\lambda$, a standard deviation $\sigma_T = \sqrt{r}/\lambda$, and their coefficient of variation is

$$CV_T = \sigma_T/\mu_T = 1/\sqrt{r}. \tag{5}$$

When $r = 1$, the GRP is the classical Poisson process. When $r < 1$, $g_T(t) \to \infty$ as $t \to 0$ and the probability of high-frequency bursts is high; the process is said to be *over-dispersed* ($CV > 1$). When $r > 1$, $g_T(t) \approx 0$ as $t \to 0$ and the probability of very closely spaced events is very low, which acts like a refractory period; the process is said to be *under-dispersed* ($CV < 1$).

When r is an integer, $\Gamma(r)$ is the factorial $(r-1)!$ and eqn. (4) is the *pdf* of the sum of r independent random variables following an exponential *pdf* with parameter λ. Put another way, in a Poisson process of rate $f = \lambda$ in which only every rth event is recorded, the intervals are distributed according to eqn. (4).

Nonhomogeneous processes

A process is said to be *nonhomogeneous* when its rate is a function of time $f(t)$. This represents the theoretical counterpart of a variable-frequency spike train. Let a new time scale τ be defined by

$$\tau(t) = \int_0^t f(u)\,\mathrm{d}u. \tag{6}$$

Intuitively, when the rate $f(t)$ is high, closely spaced events t_1 and t_2 will be mapped into event times $\tau(t_1)$ and $\tau(t_2)$ separated by a long interval, meaning a lower instantaneous frequency. Likewise, intervals (t_1, t_2) where $f(t)$ is low will be transformed into shorter intervals in the new time scale. Hence with eqn. (6), the

time axis is locally dilated or contracted to transform the time-varying process into a constant rate process.

The usual method to generate a set of event times $(t_1, \ldots, t_N)$, following the variable rate $f(t)$ (as in Fig. 1C), is to generate a realization $[\tau(t_1), \ldots, \tau(t_N)]$ of a unit rate process and map it back to the original time scale t by inverting eqn. (6).

Asymptotic behavior of the mean rate

For a general renewal process, the random variable N_t is defined as the number of events between 0 and t. The rate of the renewal process over $(0, t)$ can be estimated by the ratio N_t/t. As $t \to \infty$, the mean and variance of N_t have the following limit behavior: $E(N_t) \approx t/\mu_T$ and $V(N_t) \approx \sigma_T^2 t/\mu_T^3$ (Cox, 1962, 3.3). When the renewal process is a GRP, $\sigma_T/\mu_T = 1/\sqrt{r}$ from eqn. (5). In addition, as $t \to \infty$, the estimated rate and its variance obey the following equation:

$$\frac{V(N_t/t)}{E(N_t/t)} \approx \frac{1}{rt}. \tag{7}$$

First interval of a stationary GRP

Consider a GRP that starts at $t_0 \leq 0$. If $t_0 = 0$, then by definition, the time until the first event after $t = 0$ follows the original gamma *pdf* [eqn. (4)]; this is called the *simple* GRP. Now, if $t_0 < 0$, there may be one or more events between t_0 and 0, so the first event after $t = 0$ may no longer be the first event in the GRP. Consequently, the interval between 0 and the first event after $t_0 = 0$ will not be distributed according to eqn. (4) but to a distribution that is more complex in general, *except* in the very fortunate case where $t_0 = -\infty$; this is called the *stationary* GRP. A fundamental theorem of renewal theory (Cox, 1962, 5.2) indeed states that, in this case, the *pdf* $\tilde{g}_T(t)$ of the interval between 0 and the first event after $t = 0$ is a simple modification of the original gamma *pdf* [eqn. (4)]:

$$\tilde{g}_T(t) = \frac{1}{\mu_T}\left[1 - \int_0^t g_T(u)\,\mathrm{d}u\right], \quad t \geq 0. \tag{8}$$

Fig. 4 illustrates the difference between a simple (Fig. 4B) and a stationary (Fig. 4D) GRP. Both processes are simulated *only* between $t = 0$ and $t = 200$ ms, but the simple GRP generally shows a transient phase whereas the stationary GRP has reached steady-state right from the beginning. The stationary GRP can be seen as a simple GRP started at $t_0 \to -\infty$ and observed only after time $t = 0$, the major computational advantage being that it is not necessary to generate the full process since time immemorial.

The Poisson process is a special GRP ($r = 1$) that has the fundamental property of being *memoryless*: for any time t_0, the interval between t_0 and the first event after t_0 does not depend on the history of the process before t_0: in a Poisson process, $\tilde{g}_T(t) = g_T(t) = \lambda \exp(-\lambda t)$. Conversely, any GRP with $r \neq 1$ has memory.

When r is an integer, eqn. (8) can be simplified to the following form:

$$\tilde{g}_T(t) = \frac{\lambda}{r}\int_t^\infty \lambda \frac{(\lambda u)^{r-1}}{(r-1)!}\exp(-\lambda u)\,\mathrm{d}u$$

$$= \frac{1}{r}\sum_{k=1}^{r} \lambda \frac{(\lambda t)^{k-1}}{(k-1)!}\exp(-\lambda t). \tag{9}$$

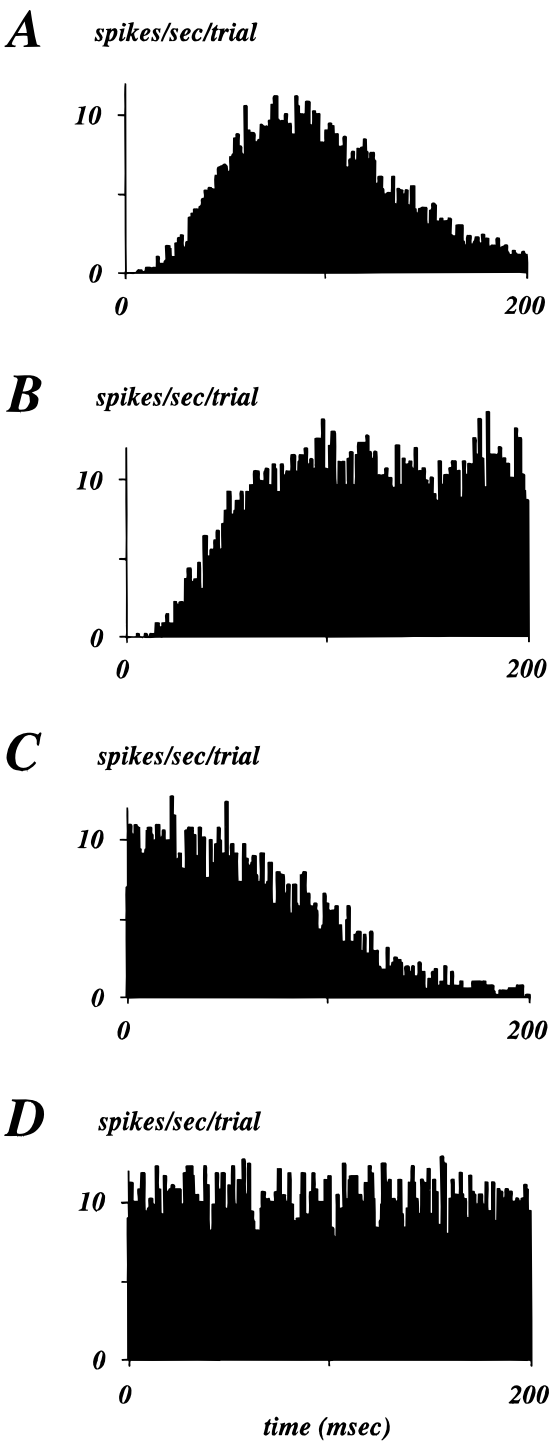

Fig. 4. Interval distributions and PSTH of simple and stationary GRPs. In the following, all processes and intervals have a rate $f = \lambda/r = 10$ spikes/s, a regularity parameter $r = 5$, and are simulated between time $t = 0$ and $t = 200$ ms ($n = 5000$). A: Histogram of the first interval in a simple GRP. The histogram is an estimation of the gamma *pdf* [eqn. (4)]. B: PSTH of a simple GRP. B differs from A in that subsequent events in the process are represented. Note that the *simple* GRP reaches a steady rate only after 80–90 ms. C: Histogram of the first interval in a stationary GRP. The histogram is an estimation of the *pdf* in eqn. (8), modified from eqn. (4). D: PSTH of a stationary GRP. D differs from C in that all events between $t = 0$ and $t = 200$ ms in the process are represented. D is called a *stationary* GRP, because its rate reaches steady-state right after time $t = 0$ ms. Bin width = 1 ms.

This has the following interpretation: the first event after $t = 0$ in the stationary GRP of parameter λ, order r and rate $f = \lambda/r$ can be the first, the second, … or the rth event in the underlying Poisson process of rate $f = \lambda$. In a simple GRP started at $t_0 \to -\infty$, the first event after $t = 0$ can be any of these r events with the same probability $1/r$.

Switching gamma renewal process

Our focus is to generate geniculate spike trains in response to a flashed stimulus, which typically involve portions of spontaneous activity, phasic discharge, and tonic discharge (e.g. Fig. 6B). The spike trains from those three episodes follow statistics of differing orders (see Discussion). Thus, we have introduced a modification of the classical GRP, named the *switching GRP*, in order to provide an easy solution to the differential modelling of those three phases within the same mathematical framework.

We define a *switching GRP* as a concatenation of *stationary* GRPs, all of which have the same mean rate. The ith GRP is defined only over the bounded interval $[t_i, t_{i+1})$ and has its own regularity parameter r_i. Importantly, at each transition time t_i, the first interval in the ith GRP is generated using eqn. (8), not eqn. (4). Subsequent intervals are generated according to eqn. (4) until the event of the ith GRP falls out of interval $[t_i, t_{i+1})$ (this event is discarded). The *nonhomogeneous* switching GRP can be constructed by mapping realizations of a unit rate switching GRP of order r back to the original time scale with eqn. (6).

An example of switching GRP is shown in Fig. 5A. Regularity in the spike train increases as r gets higher. In this example, *regularity* changes but the *rate* keeps constant. In the general case, it is possible to use both a time-dependent rate and time-dependent regularity. Fig. 5B shows a concatenation of *simple* GRPs in which the first interval after the transition in regularity (arrows) is generated with the original gamma *pdf* [eqn. (4)]; note that this process is not a switching GRP.

In the geniculate model, the set of regularity transition times for the switching GRP is a function of the frequency waveform defined as follows: $r = 1$ on intervals where the instantaneous response frequency is lower than 65 spikes/s and $r = 5$ where it is

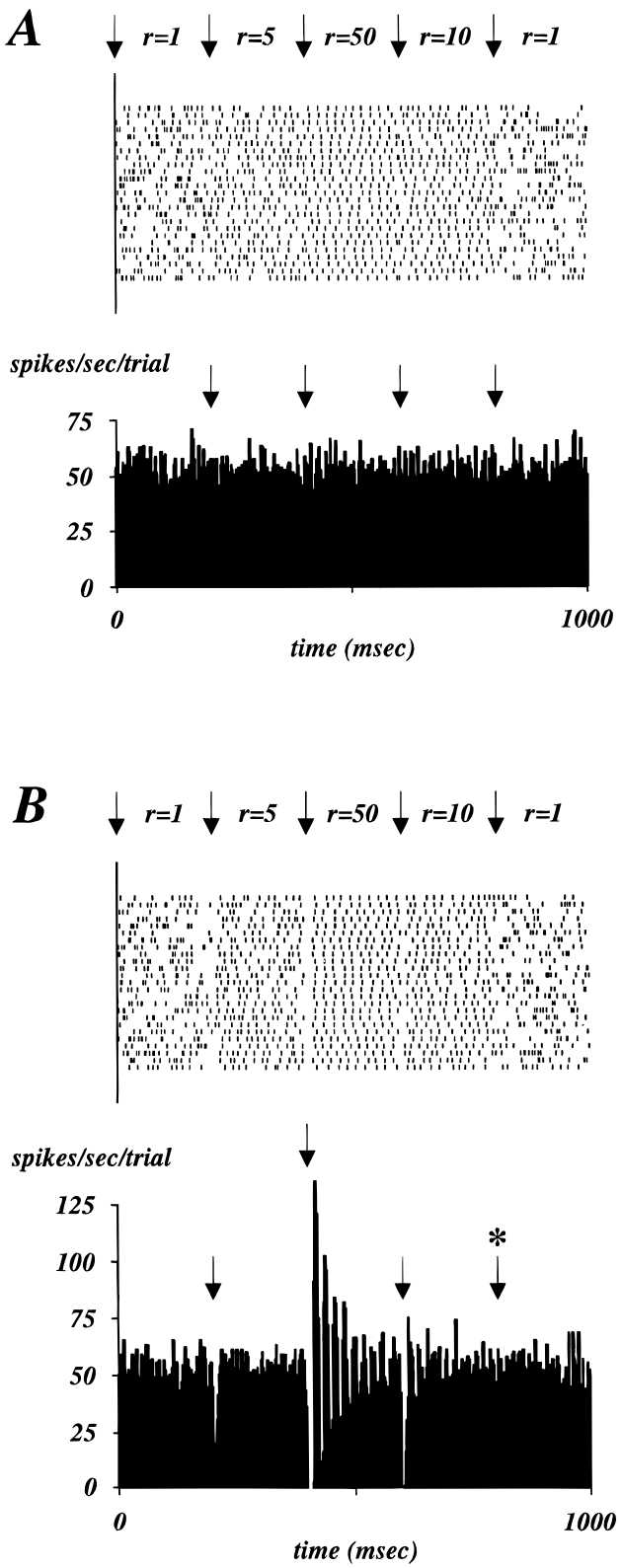

Fig. 5. Examples of switching and non-switching GRPs. A: A switching GRP with $f = 50$ spikes/s is simulated between $t = 0$ and $t = 1000$ ms. Transitions in regularity (arrows) occur every 200 ms. Raster plot shows the first 25 single realizations of the switching GRP, aligned on time $t = 0$ ms. The histogram compiles 500 realizations of the switching GRP, including the 25 displayed. At each transition time, the first interval is generated with the *modified* gamma *pdf* [see eqn. (8) and Fig. 4C]; subsequent intervals are generated with the classical gamma *pdf* [eqn. (4)]. The higher the regularity r, the more intervals tend to be concentrated around their mean duration. When $r = 1$, the switching GRP is statistically equivalent to a Poisson process. Using the modified gamma *pdf* makes the transition between different regularity periods very smooth. The histogram estimates f very closely; there is no sign in the histogram which reveals the underlying transitions in regularity. Bin width = 2 ms. B: A concatenation of GRPs is simulated with the same conventions and characteristics as in A, *except* that the first interval after a regularity transition is generated with the *original* gamma *pdf* [see eqn. (4) and Fig. 4A]. This process is thus not a switching GRP. In this case, transitions in regularity are obvious in the histogram (first three arrows). Dips at the first and third arrows correspond to the slow rise of Simple GRPs (Fig. 4B). The oscillatory pattern (second arrow) is due to the high regularity ($r = 50$) of spike trains and their reproducibility from trial to trial in this portion. At the beginning of the Poisson portion (arrow with asterisk), the switching and non-switching case are statistically identical.

higher (see Discussion). Different frequency waveforms have different sets of regularity transition times, in general.

Model structure for OFF-center nonlagged X-cells

We have assumed symmetry between ON-center and OFF-center geniculate RFs, but the alterations of Fig. 2 to transform the ON-center model into an OFF-center one are straightforward: nonlinearities are flipped about the *y* axis. Hence, functions become $\Psi(-x)$ in C1,C3; $-\Psi(-x)$ in C2,C4; $-\Psi(x)$ in C5,C7; and $\Psi(x)$ in C6,C8. This transformation means that spatio-temporal filters will play the same functional role, but for the opposite contrast. Other parameters are unchanged.

Simulation software

The simulations were carried out using the Surf-Hippo 2.7 neuron simulator package (Borg-Graham, 1997), on a SPARCstation 5 running Solaris 2.4. Code is available by ftp from cogni.iaf.cnrs-gif.fr. We used the random number generator provided with the CMU Common Lisp environment, version 18a.

Results

In this section, we describe how we extracted the parameters of the model from the electrophysiological literature. Whenever possible, we tried to compare the experimentally derived estimates provided by several authors and different protocols.

Spontaneous activity

Spontaneous activity is a random discharge that occurs in LGN cells when they are subjected to no visual stimulation other than a uniform background luminance. An overestimation of this quantity may result in unstable "resting" states in the cortical network; an underestimation may decrease the excitability and integrative properties of whichever cells receive the geniculate background synaptic noise. Spontaneous activity can also be envisioned as a mean level that the visual signal can modulate up and down (Kuffler et al., 1957).

A reference level for spontaneous activity is very difficult to define since, in the general case, it depends on the visual adaptation level of the retina (Kaplan et al., 1979), on the arousal state of the animal (Sakakura, 1968; Livingstone & Hubel, 1981) and on the anesthetics (Levick & Williams, 1964). We have chosen to model a physiological state close to the usual experimental preparation: an anesthetized animal in the mesopic ambient luminance range (0.1 to 25 cd/m^2, Hammond & James, 1971).

The estimates of spontaneous activity in geniculate X-cells provided by several authors have been summarized in Table 1. As assessed by these results, a spontaneous discharge frequency of 10 spikes/s seems in the physiological range. This is the value we chose for both ON- and OFF-center X-cells in the model.

Receptive-field center size

The average RF center size increases from the *area centralis* to the visual-field periphery (Hubel & Wiesel, 1961). In our model, the center size is defined as the diameter of the centered spot eliciting maximum response. Pooling all eccentricities and cell types, the RF center diameter varies between 0.3 and 2.0 deg in the light-adapted state (Virsu et al., 1977). The apparent RF center size has a tendency to widen in the dark-adapted state (Virsu et al., 1977), up to threefold (Kaplan et al., 1979). A comparison of estimates of the mean RF center size provided by various authors is given in Table 1. We chose 0.5 deg as the RF center diameter of our generic X-cell, which corresponds to the average RF center diameter for X-cells with a single retinal afferent at an approximate eccentricity of 6.0 deg, in the mesopic background luminance domain. Together with the constraint on CSA (see below), this choice could be satisfied by setting the space constant of the center Gaussian to $\sigma_{in} = 0.11$ deg and that of the surround gaussian to $\sigma_{out} = 0.33$ deg.

Phasic and tonic responses to an optimal spot

When a small light spot is flashed in the center of an ON-center cell, the cell first responds with a short high-frequency phasic discharge, followed by a longer tonic discharge. The phasic discharge in response to an optimal spot lasts about 50 ms on the spatio-temporal maps of Bullier and Norton (1979, Fig. 2C). The primary excitation described by Singer and Creutzfeldt (1970) was reported to last about 30 ms, but this might be an underestimation of the transient peak due to a pronounced secondary inhibition (transient suppression between the phasic and the tonic responses,

Table 1. *Center size and spontaneous activity derived from the experimental literature*[a]

References	Eccentricity (deg)	Center size (deg)		Spontaneous activity (spikes/s) ON-center	Spontaneous activity (spikes/s) OFF-center
Bullier & Norton (1979)	<10.0	0.51		7.8 ± 4.6	8.0 ± 4.2
Wilson et al. (1976)	All	0.5 (0.3–1.0)		2.5–12.5	0.0–7.5
Hoffmann et al. (1972)	3.0–10.0	0.67		—	
Sanderson (1971)	4.0–8.0	0.8–0.9		—	
Saul & Humphrey (1990)	Around 10.0	0.7 (0.2–2.0)		—	
Teich et al. (1997)	—	—		6.6	
Levine & Troy (1986)	—	—		15	
		XS	XM	XS	XM
Mastronarde (1992)	Around 6.0	0.51	0.87	11 ± 7	11 ± 9

[a]This table summarizes the average center size (in deg) and the mean spontaneous activity (in spikes/s) for X-cells at different eccentricities. Spontaneous activity in Bullier and Norton (1979) and Mastronarde (1992) are means ± S.D. XS: single-afferent X-type relay-cell; and XM: multiple-afferent X-type relay-cell.

see Discussion). In the impulse response given by a difference of exponentials [eqn. (2)], we chose values of $\tau_1 = 13$ ms and $\tau_2 = 15$ ms, yielding a width at half-height of 38 ms in the phasic waveform.

Humphrey and Weller (1988, Fig. 6) have provided a distribution of the peak frequency during the phasic discharge of nonlagged X-cells in response to spots 60% larger than the center. This might have underestimated the maximal response because of center/surround antagonism. The rates ranged between 50 and 400 spikes/s, with a mean of 161 spikes/s (contrast $\Delta L/L = 0.6$). Saul and Humphrey (1990) reported a slightly lower estimate (131 spikes/s) but with lower contrast ($\Delta L/L = 0.4$). In addition, there is indication that the peak phasic discharge may actually be higher for multiple-input (275 ± 89 spikes/s) than for single-input X-cells (157 ± 83 spikes/s), in response to an optimal spot (Mastronarde, 1992). Taking 160 spikes/s as a first approximation to the peak phasic discharge frequency seems a reasonable value for nonlagged X-cells with a single retinal input.

Is there a relationship between phasic and tonic discharge levels in a given cell? Bullier and Norton (1979) have defined the phasic/tonic index as the ratio of the tonic discharge to the peak phasic frequency (spontaneous activity subtracted). This index was estimated to 34 ± 18%, which gives a tonic discharge of 61 spikes/s, assuming a spontaneous discharge level of 10 spikes/s and a peak phasic discharge of 160 spikes/s. Similarly, Saul and Humphrey (1990) computed the ratio of mean to maximal discharge, without subtracting spontaneous activity. This ratio was 38 ± 16% for nonlagged X-cells and gives a tonic discharge of 60.8 spikes/s, consistent with the above study.

We therefore decided that in our model the response of a nonlagged X-cell to an optimal centered spot, at the fixed level of contrast that we have chosen, would consist of a phasic discharge of 160 spikes/s, followed by a tonic discharge of 60 spikes/s (Fig. 6B). This allowed to constrain the impulse response amplitudes *A* and *B* [eqn. (2,3)] on the "positive contrast" half of Fig. 2 (*A* in B1–B2 and *B* in B3–B4). These parameters are closer to the behavior of single-input X-cells than multiple-input X-cells, but this choice seems justified in that single-input X-cells dominate in the neighborhood of the *area centralis* (Mastronarde, 1992).

Center/surround antagonism

When a small light spot is flashed over the RF center, the response is initially weak. As the spot diameter increases, the response grows because of spatial summation in the center. When the spot is enlarged so as to encroach on the surround, the cell responds less strongly; this is referred to as center/surround antagonism (Hubel & Wiesel, 1961; Hammond, 1973; Bullier & Norton, 1979).

The degree of CSA is all the more pronounced as (1) the cell is further away from the *area centralis* (Hubel & Wiesel, 1961), and (2) the RF center is small (Hammond, 1973; Bullier & Norton, 1979). As stated earlier, there is considerable experimental evidence that RF surrounds are more potent in antagonizing the center excitatory responses in geniculate cells than in retinal ganglion cells (Maffei & Fiorentini, 1972; Hammond, 1973; Bullier & Norton, 1979; Sillito & Kemp, 1983; Cleland & Lee, 1985). Sillito and Kemp (1983) have shown that this is at least partially due to intrageniculate GABAergic inhibition, since iontophoresing the $GABA_A$ receptor antagonist bicuculline reduced the degree of geniculate CSA to values observed at the retinal level.

Many examples in the literature give quantitative indications as to the level of CSA in the LGN. Bullier and Norton (1979, Fig. 8A) show an X-type RF whose center diameter is 0.4 deg, and whose response is totally suppressed for a stimulus 2.4 deg in diameter. In Fig. 4 of Hammond (1973), the RF center is about 2.0 deg wide, and the response falls to 10% of optimal for a spot diameter of 8.0 deg. Likewise, Hammond (1972, Fig. 7A) shows a cell with a RF center 0.75 deg in diameter and a response 10% of maximal at a spot diameter of 3.0 deg. Another example from Sillito and Kemp (1983, Fig. 8) is an ON-center X-cell with a center diameter of 0.5 deg with a response 5% of maximal at a spot diameter of 2.0 deg.

These data may be reasonably summarized by considering that the response to a centered spot with a diameter four times as large as the center is less than 10% of the optimal spot response (criterion 1). This conclusion has been drawn from a collection of isolated examples because we could not find an estimation (based on a large sample of cells) of what the spot size should be to get a fixed reduction (e.g. 90%) of the optimal spot response, except in Hammond (1973): for cells with an RF diameter of 0.5 deg, he estimated the discharge would fall to 60% of maximum for spot diameters of 0.8–0.9 deg (criterion 2).

We found that both criteria could be met by considering a simple difference of iso-volume bidimensional Gaussians: the peak phasic response to a 0.9-deg spot is 99 spikes/s, namely 62% of the peak phasic discharge in response to an optimal centered spot (0.5 deg, 160 spikes/s). Moreover, with this choice, the peak phasic response (including spontaneous activity) to a 2.0-deg spot diameter is 8% of maximum. Following Hammond (1972), we assume that the same degree of CSA exists for the phasic and tonic responses. The iso-volume assumption translates into using the same impulse responses in each pair of antagonistic center/surround filters (Fig. 2, row B).

Fig. 6 shows the behavior of the model in an expanding spot protocol. The small spot in Fig. 6A covers only part of the RF center, yielding a suboptimal response. Fig. 6B is the optimal spot response described earlier. The phasic discharges in Figs. 6A, 6B, and 6C are generated using the high-regularity GRP ($r = 5$), because the frequency is above 65 spikes/s; all other portions of the responses are generated by Poisson processes ($r = 1$, see Discussion). Figs. 6C and 6D show how responses get weaker when the spot covers part of the surround.

Cleland and Lee (1985, Fig. 4) show the differential CSA between a single geniculate cell (RF center diameter, 0.65 deg) and its main retinal ganglion cell afferent: in a nonlagged geniculate X-cell, the response to a 2.5-deg spot is almost brought down to the spontaneous level, whereas the same response has barely decreased from the optimal spot response in the main retinal afferent. Fig. 7 summarizes the comparative performance of the retinal model used in Somers et al. (1995) together with our work and the typical data from Sillito and Kemp (1983, Fig. 8).

Excitatory responses from the surround

It is known that geniculate RF surrounds are not only capable of antagonizing the center's excitatory responses but also of producing themselves a discharge in response to annuli or spots of the proper contrast (Hubel & Wiesel, 1961, Fig. 1D; Singer & Creutzfeldt, 1970, Fig. 4; Sillito & Kemp, 1983, Figs. 2 and 3; Cleland & Lee, 1985).

Spatial summation occurs in the surround too. When the inner diameter of a light-centered annulus that initially covers only the far OFF-surround decreases, the excitatory response at light OFF increases (Cleland & Lee, 1985, Fig. 7B). When the inner diameter

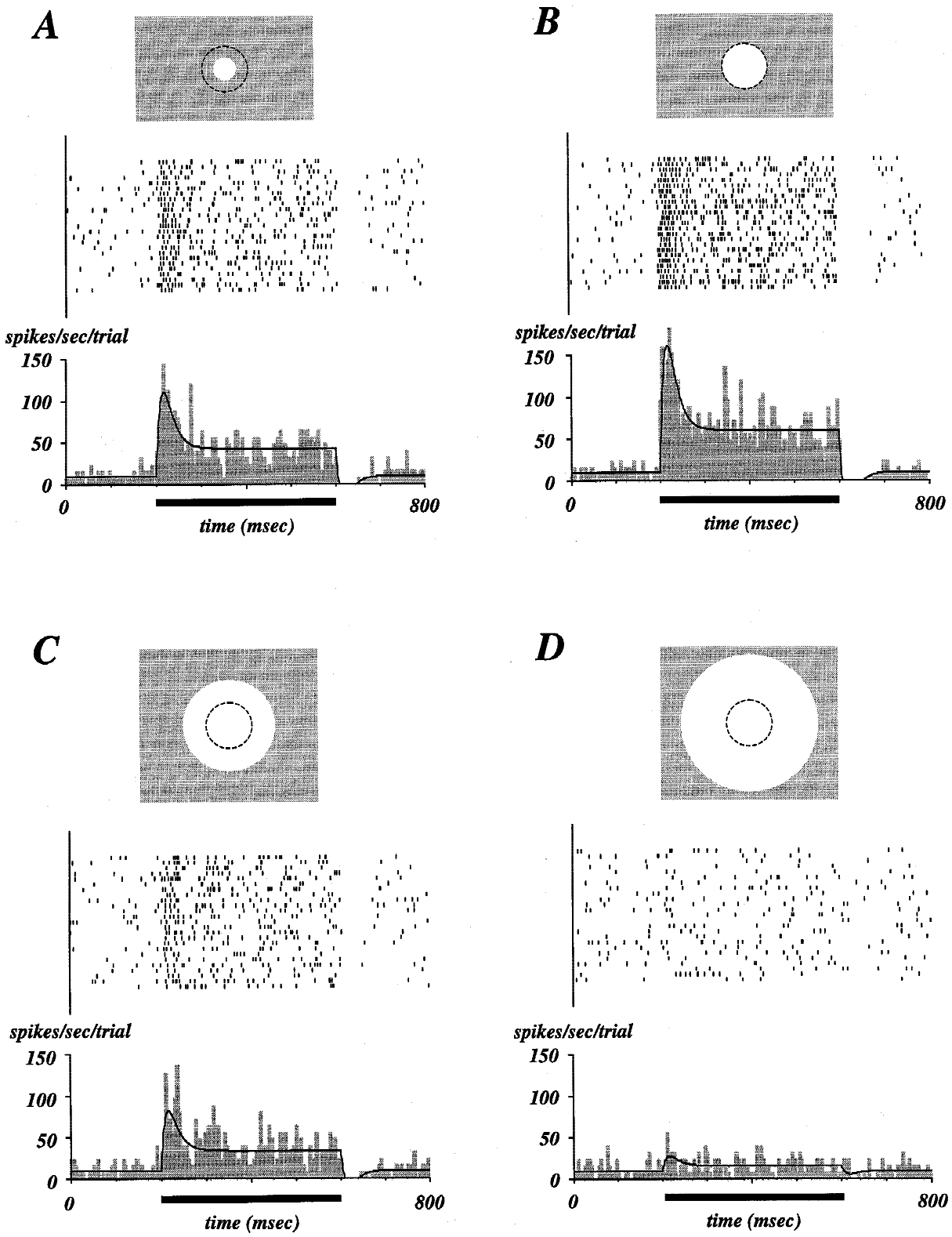

Fig. 6. Simulated expanding spot protocol. This figure shows the responses of a model geniculate nonlagged ON-center X-cell to centered spots of expanding diameter and positive contrast. RF center diameter is 0.5 deg (dashed circle). Light spots are represented as white disks. On this figure and the following, background luminance is represented as a grey rectangle. This rectangle is represented as finite but should be seen as spanning the whole visual field. Spot diameter is 0.25 deg in A, 0.5 deg in B (optimal stimulus), 1.0 deg in C, and 1.5 deg in D. In all plots, the stimulus is presented at $t = 200$ ms and disappears at $t = 600$ ms (black bar). Histograms are compiled from the 25 spike trains shown above. The continuous line represents the ideal frequency waveform from which the spike trains are generated. A–D: Bin width = 5 ms, contrast $I = 1.0$. Peak phasic discharge level (spikes/s): A, 110; B, 161; C, 82; D, 27. Tonic discharge level (spikes/s): A, 43; B, 60; C, 34; D, 16.

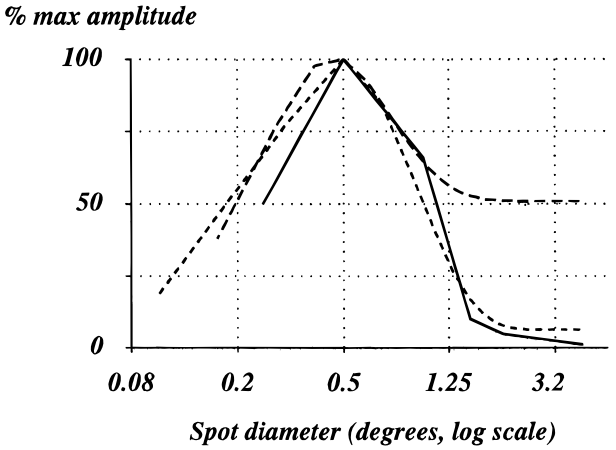

Fig. 7. Comparative center/surround antagonism levels. Discharge levels are measured in response to centered spots of varying diameters. Response amplitudes normalized to the maximum response are plotted versus spot diameter (log coordinate along *x)*. *Solid line* is the curve plotted in Sillito and Kemp (1983, Fig. 8); this curve was chosen since the cell has properties very close to the specification of our model: it is a (probably nonlagged) geniculate ON-center X-cell with an RF center size of 0.5 deg. *Short dashed line* shows the center/surround antagonism behavior of the model described in this paper, very close to the experimental data of Sillito and Kemp (1983). *Long dashed line* shows the center/surround antagonism of the retinal model by Somers et al. (1995); the level is adequate at spot diameters up to 1.0 deg, but the surround is much less efficient at antagonizing the center excitatory response at larger diameters.

of the annulus becomes smaller than the RF center diameter, the response decreases, meaning that the center also exerts antagonism on the surround response (Cleland & Lee, 1985, Fig. 6B).

The stimulus used to measure surround responses is usually an annulus that optimally covers the surround. The outer diameter of this *optimal* annulus is very large and its inner diameter is the RF center diameter. With such a protocol, Cleland and Lee (1985, Figs. 7A, and 7B) showed that peak phasic surround responses can be very similar in amplitude to optimal centered spot responses. The excitatory strength of surrounds is extremely variable from cell to cell; indeed, Horton and Sherk (1984, Fig. 6) found that the ratio of the optimal annulus response to the optimal spot response could vary between 0% and 100%, occasionally rising above 100%, with an average of 45%.

We assume in the model that the presentation of a dark annulus in the OFF-surround of an ON-center cell also produces a phasic and a tonic discharge, the amplitude of which can be scaled from the optimal spot response by applying the proportionality factor (45%) found by Horton and Sherk (1984). The response to a dark optimal annulus thus consists of a peak phasic discharge of about 78 spikes/s, and a tonic discharge of about 33 spikes/s (spontaneous activity included).

This data allows to calibrate the impulse response amplitudes A and B in the right half of Fig. 2 (A in B5–B6 and B in B7–B8). Fig. 8A shows the response of an ON-center RF model to a dark optimal annulus flashed above the OFF-surround. Fig. 8B illustrates the response to a light annulus; an initial suppression is followed by a phasic discharge at the OFF transition.

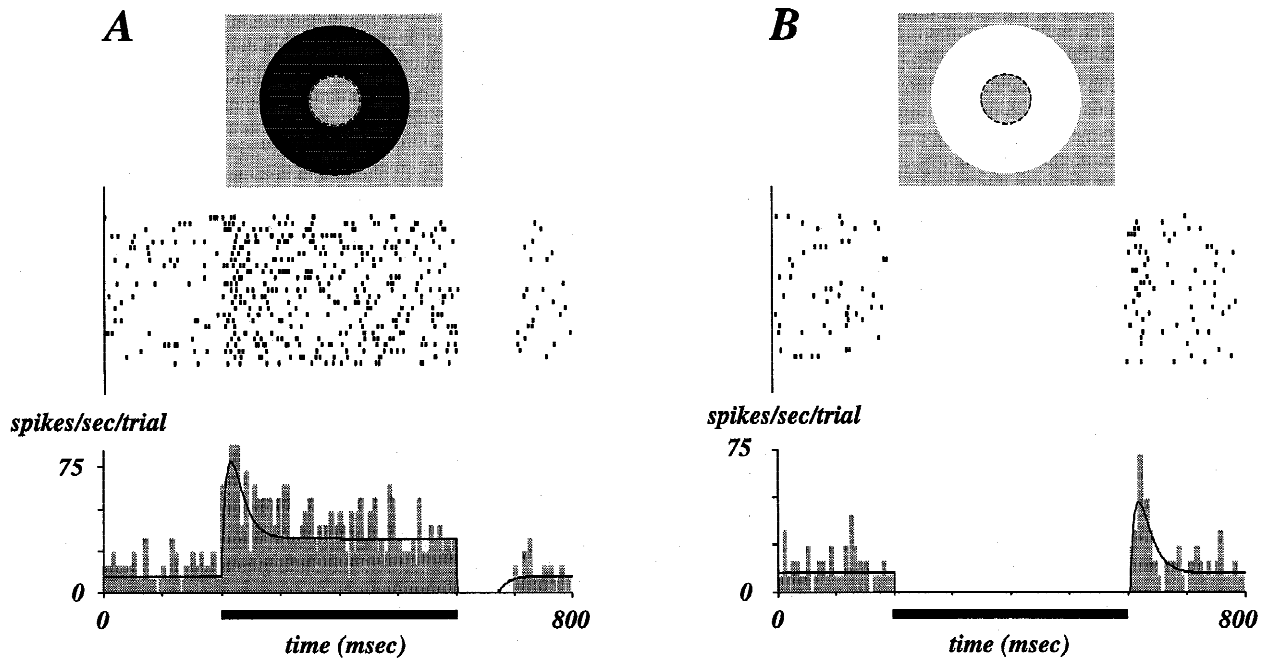

Fig. 8. Model responses of an ON-center cell to light and dark optimal annuli. An optimal annulus has an inner diameter equal to the RF center diameter (0.5 deg), and an infinite outer diameter (represented as finite, for obvious reasons). This is the stimulus that can evoke the maximum response from the surround. A: A dark optimal annulus (black annulus) is flashed above the OFF-surround. Presentation evokes an excitatory response. Peak phasic response, 78 spikes/s; tonic response, 32.5 spikes/s. Contrast $I = -1.0$, $n = 25$. B: A light optimal annulus (white annulus) is flashed above the OFF-surround. Annulus presentation suppresses spontaneous discharge; withdrawal evokes a phasic response only. Peak phasic response, 47 spikes/s. Contrast $I = 1.0$, $n = 25$. Other conventions are as in Fig. 6.

Generalizing the model to bar responses

Modelling geniculate responses to flashed bars is important since studies of cortical visual responses often use such stimuli. The visual responses to flashed bars shown in Figs. 9 and 10 differ from the model responses shown so far (optimal spot responses and optimal annulus responses) in that they have not been used to design the model or to constrain its parameters. They represent a test of the model on a new kind of visual stimulus. The generalization to a new kind of stimulus geometry is critically dependent on the assumption of linearity in the spatial summation properties of geniculate RFs (see Discussion).

To our knowledge, the only examples of geniculate responses to bars flashed in the surround are provided by the spatio-temporal

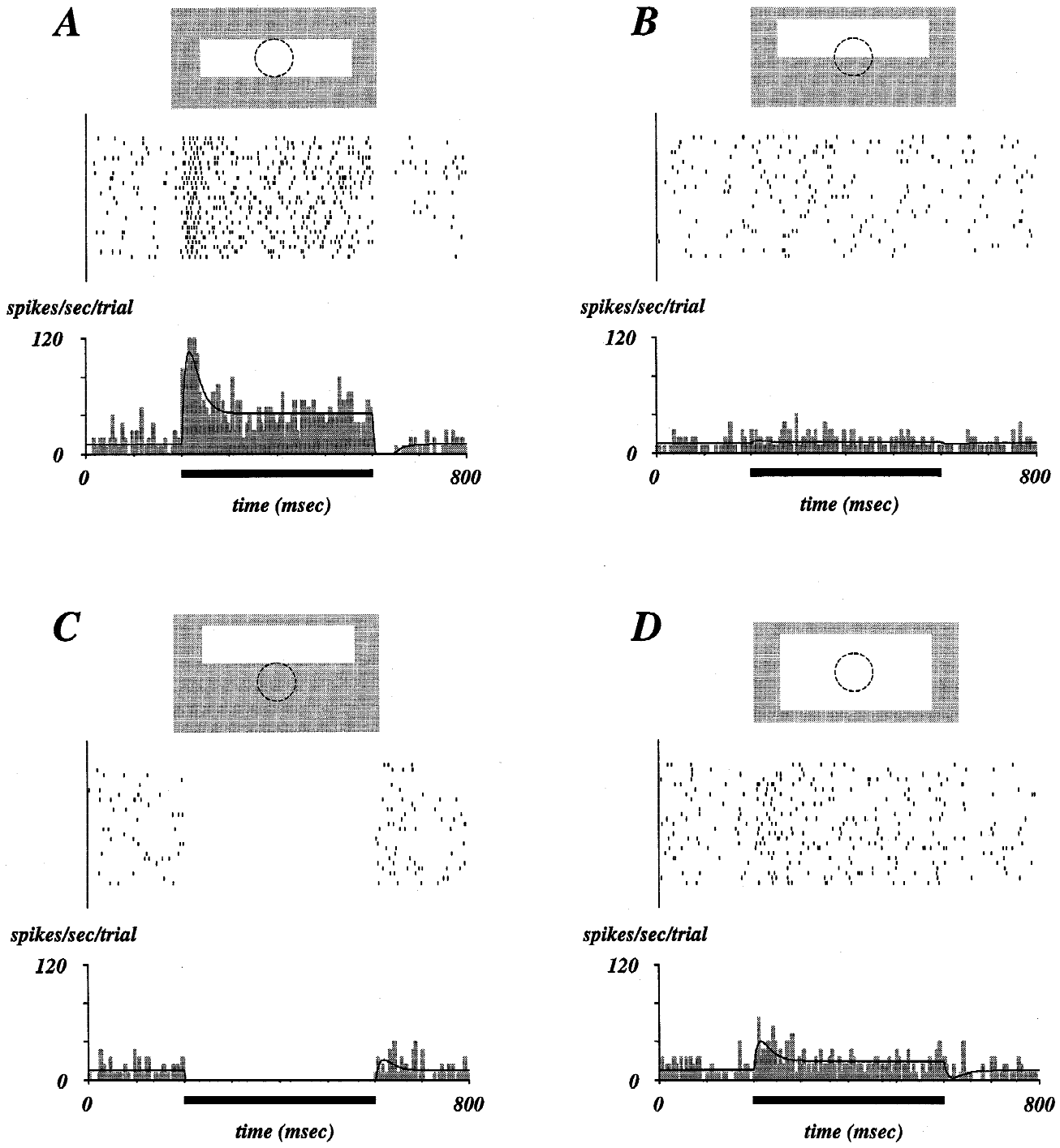

Fig. 9. Response to light bars flashed in various RF positions in the model geniculate nonlagged ON-center X-cell. Bar dimensions: A–C, 0.5 × 2.0 deg. D, 1 × 2 deg. Peak phasic response (in spikes/s): A, 106; B, 12.5; C, 21 (at light OFF); D, 40. Tonic response (in spikes/s): A, 42; B, 10.8; C, no tonic response; D, 20 (see text). Contrast $I = 1.0$, $n = 25$. Other conventions are as in Fig. 6.

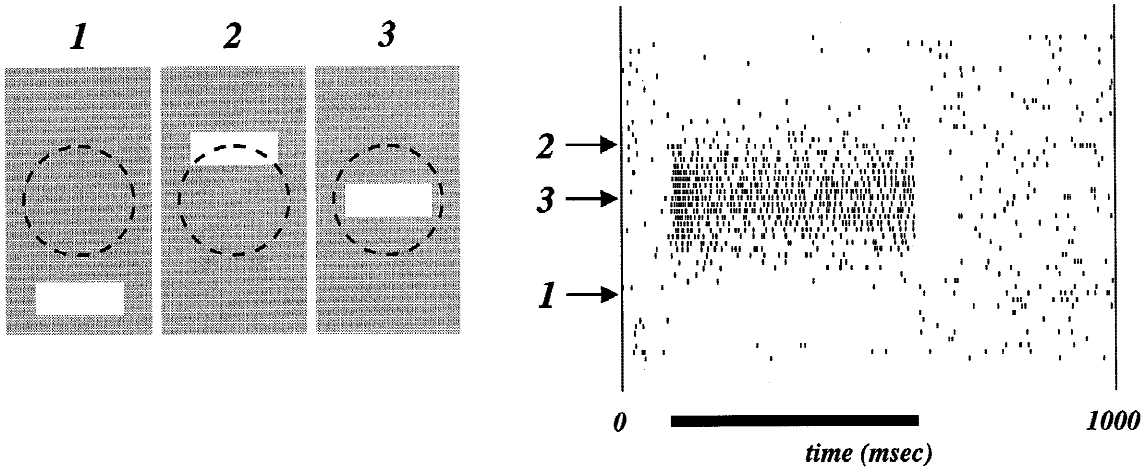

Fig. 10. Simulated spatio-temporal map in the model geniculate nonlagged ON-center X-cell. A thin light bar was flashed in 51 overlapping positions across the receptive field. Each response is displayed as a raster. The stimulus positions span 1.5 deg, that is three times the RF center diameter. On the left, relative locations of the stimulus and the receptive-field center are shown for three stimulus positions. The bar and the receptive-field center are drawn at the same scale. The shaded rectangle represents the background luminance. Light bars are flashed ON at $t = 100$ ms and OFF at $t = 600$ ms. Receptive-field center diameter, 0.5 deg. Bar dimensions, 0.4×0.15 deg. Step between two positions, 0.03 deg. Note that contrast $I = 3$ here. Other conventions are as in Fig. 6.

maps of Bullier and Norton (1979) and the results of Tanaka (1983, Figs. 7, and 8). The spatio-temporal maps use thin bars in order to estimate the RF sensitivity profile precisely, at the cost that they may not be able to evoke significant excitation from the surround. On the other hand, the bars used by Tanaka (1983) are of the size typically used when studying cortical RFs.

Both protocols were simulated in the model and yield results similar to the experimental findings. Fig. 9A shows the response to a light bar flashed in the RF center, and this strong response is comparable to that shown by Tanaka (1983, Figs. 7D and 8D). When flashed in the OFF-surround (Fig. 9C), the light bar completely suppresses the geniculate response with a little discharge at light-OFF. This is similar to the result of Tanaka (1983, Fig. 7F). Fig. 10 shows a simulated spatio-temporal map. The bar dimensions and shift were adjusted as in Bullier and Norton (1979), with a bar length 0.8 times the RF center diameter and a width 0.3 times the RF center diameter. Since the bars are much smaller than in Fig. 9, contrast I was increased up to 3.0 to produce a stronger response. The overall spatial pattern of excitatory responses and suppressions in the simulations look very similar in many respects to the experimental X-cell maps (Bullier & Norton, 1979, Figs. 2, 3, and 5A–5C). Phasic responses have the same lateral extent as tonic responses, which was claimed to be a distinguishing feature of X-cells.

Tanaka (1983, Figs. 7D and 7F) shows a cell whose response to a bar flashed in the surround is only 10% of the response to the same bar flashed in the RF center. The ratio is 20% in our model (106 *versus* 21 spikes/s, Figs. 9A and 9C). Note that the cell shown by Tanaka (1983, Fig. 7F) has a phasic (but no tonic) suppression of spontaneous activity in response to a light bar flashed in the OFF-surround, whereas tonic suppression is complete in our model (Fig. 9C; Fig. 10, position 1). The results by Bullier and Norton (1979) are intermediate. It is not known whether Tanaka's situation is typical and, in any case, the experimental literature really does not give enough quantitative data yet to suggest differential modelling of the phasic and tonic surround suppression.

Discussion

The main result brought by this model is an operational method for generating geniculate spike trains in response to flashed spots and bars. The receptive-field part of the model has been constrained according to the visual properties of cat geniculate nonlagged X-cells. The spike train generation mechanism has been designed to fit the statistical properties of spontaneous and visually evoked geniculate firing. The resulting model can be used to generate a more realistic input to a cortical network than classical retinal models.

Essential differences with retinal models

Geniculate X-cells differ from retinal ganglion X-cells in their level of spontaneous activity, relative phasic and tonic response amplitudes, spike train statistics and the existence of burst firing, and the level of center/surround antagonism. So far, cortical modelling studies (Wehmeier et al., 1989; Wörgötter & Koch, 1991; Somers et al., 1995; Maex & Orban, 1996) have resorted to retinal ganglion cell models to provide visual excitation to the cortical network since no operational geniculate X-cell model was available.

In severals respects, our geniculate model is different from the usual retinal models and modifying the latter in minor ways could not overcome their fundamental limitations. First, within the X pathway, the retino-geniculate projection is usually one-to-one, with a transfer ratio in anesthetized preparations rising from low values during spontaneous activity up to 80% in response to drifting gratings of optimal temporal frequency (Hamamoto et al., 1994) and up to 100% during phasic responses to flashed spots (Hartveit & Heggelund, 1995). Under these visual stimulation conditions, excitatory postsynaptic potentials (EPSPs) are so powerful that almost all retinal spikes elicit a geniculate spike. In contrast, geniculo-cortical projections involve some degree of convergence (Tanaka, 1983) and *strong phasic discharges* are needed from a number of presynaptic geniculate cells to drive the cortical target

cell. Therefore, modelling the phasic discharge with the right frequency and the right regularity is critical in having the necessary number of spikes to evoke a response from the cortical network. However, our preliminary simulations of the cortical network show that if the amplitude of the tonic geniculate response is not significantly attenuated relative to the phasic input, as is the case for retinal models, then the network will receive too much tonic excitation and be driven into an unrealistic state of activity. For this reason, it is fundamental to dissociate the amplitudes of phasic and tonic discharges, which we did by splitting the filters into a phasic set and a tonic set.

Second, in the model that we propose, center/surround antagonism is quantitatively close to its experimentally measured level. In particular, geniculate surrounds are strong enough to antagonize center responses to large centered spots, which is of major importance in a model of the ON/OFF organization of simple receptive fields. While it is true that retinal models could be modified in minor ways to account for the level of CSA found in the LGN, they cannot account for the amplitude of the surround excitatory responses and their intercell variability. Indeed, in retinal models, the response to a light spot flashed in the center and the response to a dark annulus flashed in the surround cannot be constrained separately because these models are made of only two spatio-temporal filters. The exact level of surround excitatory responses has always hindered investigators from interpreting the origin of distinct subregions within the same cortical simple RFs and from distinguishing the relative influence of the thalamo-cortical and intracortical mechanisms. Also, in a given geniculate cell, the optimal annulus response can be any percentage of the optimal spot response. Should this intercell variability be ever included in the thalamic stage of a cortical model, it could not be if the model does not allow some fine differential tuning of the center and surround excitatory responses. Accordingly, we have split the filters for center and surround responses.

Lastly, more sophisticated models of spontaneous geniculate firing have been proposed (Levine & Troy, 1986; Teich et al., 1997) but the issue of visual responses was left apart. In these studies, spontaneous activity was modelled over long periods of time (≈80 min), whereas we focus on a much shorter time scale (≈1 s), neglecting the hidden long-term temporal structure. The switching GRP method (see below) allows to model spontaneous and visually evoked spike trains within the same mathematical framework.

Spatial dependence of visual inhibitory input

At the retinal level, circular Gaussians have been shown to provide excellent fits to the spatial dependence of both center and surround influences (Rodieck, 1965; Enroth-Cugell & Robson, 1966). In the LGN, there is still controversy about the exact shape of the inhibitory input, with some authors claiming that it also has a Gaussian profile, and others arguing that it looks more like a doughnut. Singer and Creutzfeldt (1970) have shown with quasi-intracellular recordings that inhibitory visual input to the geniculate cell increased when a small spot was flashed further away from the RF center. However, Coenen and Vendrik (1972) have observed that hyperpolarizations were present even in responses elicited by stimulation of the center only. Besides, simultaneous recordings of both retinal inputs (S-potentials) and cell output (spikes) have shown that for small spots covering only part of the center, geniculate response was already weaker than the retinal input signal (Cleland & Lee, 1985; Fjeld et al., 1997) and the transfer ratio was lower than one, suggesting that visually driven geniculate inhibition is already effective across the RF center.

Therefore, we modelled the surround with a circular Gaussian. Doing so introduces just one parameter, the standard deviation σ, which is easy to calibrate with center-surround antagonism, whereas a doughnut profile would need two parameters. In addition, the numerical integration with a Gaussian is made very efficient by eqn. (A1).

Linearity in the spatial domain

Linearity in the dependence of the response on the stimulus shape is a major assumption in our model, as it was in earlier retinal models. If the cell is known to behave linearly, its response to any stimulus geometry can be predicted from the responses to more simple patterns. This assumption of linearity has been shown to be valid for X-cells with the method of the bipartite field (Kratz et al., 1978; Bullier & Norton, 1979) or the method of contrast reversal gratings (So & Shapley, 1979).

Postphasic suppression

Some authors describe a "secondary inhibition," or "postphasic suppression" between the phasic and tonic discharge (Singer & Creutzfeldt, 1970; Coenen & Vendrik, 1972, Fig. 2; Hammond, 1973; Virsu et al., 1977). Yet, it is noted elsewhere that this suppression disappears during dark adaptation (Virsu et al., 1977), that for nonlagged X-cells it is only present at high stimulus contrasts (Hartveit & Heggelund, 1992), and that above all this suppression may be dependent on the anesthetic employed (Cleland & Lee, 1985). Therefore, this characteristic was not incorporated in the model.

Contrast dependence

The parameters we found are valid at relatively low contrasts. At higher contrasts, nonlinear behaviors appear and responses saturate (Cleland & Lee, 1985; Hartveit & Heggelund, 1992). Flashing higher contrast stimuli presumably evokes a more significant contribution from intra-geniculate inhibition; therefore, modelling network effects may be necessary to account for the contrast dependence of the response in the general case. Geniculate network effects were neglected here because we wanted to keep the model at the same phenomenological level as earlier ganglion cell models (Rodieck, 1965; Linsenmeier et al., 1982; Richter & Ullman, 1982) in particular for application to large-scale neural simulations (e.g. Somers et al., 1995; Maex & Orban, 1996).

Correlations between geniculate cells

It has recently been shown that neighboring geniculate relay cells exhibit correlated firing on a fast time scale in response to visual stimulation (Alonso et al., 1996). Indeed, the transfer ratio between retinal input and geniculate spike output is close to one and neighboring retinal ganglion cells themselves have correlated firing (Mastronarde, 1983). A retino-geniculate divergence factor higher than one might also explain correlations between geniculate cells fed by the same axon. Coincidence in the discharge of presynaptic geniculate cells might enhance their ability to bring the cortical target cells to threshold.

In our model, it is possible to incorporate correlations on a fast time scale between the spike trains of cells whose RFs are of the same center type and overlap, in a straightforward way. When RFs overlap, the frequency waveforms $f(t)$ computed for both cells are equal for any stimulus and hence, the mappings described in eqn. (6) are identical. Generating two correlated switching GRPs that meet the frequency requirement of $f(t)$ in the original time scale amounts to generating two correlated unit-rate Poisson processes in the transformed time scale. For example, two unit-rate Poisson processes with a 25% correlation can be generated by simply superposing a common Poisson process of rate 0.25 Hz with two independent Poisson processes of rate 0.75 Hz. The correlated variable-rate switching GRPs are then obtained by mapping the correlated Poisson processes back into the original time scale, inverting eqn. (6) which, again, is identical for both cells.

Stimulus dependence of visual latencies

Interactions exist between latency to spike discharge and the type of visual stimulus: discharge latency seems to decrease when a centered spot grows as to cover the whole RF center (Bullier & Norton, 1979, Fig. 8) or when the stimulus contrast is raised (Hartveit & Heggelund, 1992). However, the latency of the primary excitation and secondary inhibition do not change when a small light spot is flashed progressively further away from the RF center (Singer & Creutzfeldt, 1970). While visual latency seems to be negatively correlated with peak phasic discharge (Humphrey & Weller, 1988), Sestokas et al. (1991) report that visual latency in the LGN is not a straightforward function of amplitude or contrast. Our preliminary simulations have shown that an explicit dependence of discharge latency on stimulus location in the LGN model is not necessary to account for a large body of experimental data on the RF organization of cortical simple cells. Consequently, the delay between the stimulus presentation and the beginning of the firing was set to zero in all cases, irrespective of response amplitude, stimulus contrast, or stimulus position.

Relevance of switching GRPs

Is it legitimate to model geniculate spike trains with renewal processes? It has been shown that, during spontaneous activity, the sequences of interspike intervals (ISIs) derived from geniculate spike trains have a hidden temporal structure (Levine & Troy, 1986; Teich et al., 1997) such that dependencies exist between nearby intervals (for example, an interval longer than average tends to be followed by an interval shorter than average). On the other hand, the intervals generated by a renewal process are by definition independent. Therefore, strictly speaking, renewal processes are not appropriate to model spontaneous geniculate spike trains.

However, the GRP is attractive because it is mathematically simple, depends only on two parameters λ and r, and provides reasonable fits in most cases (Teich et al., 1997). The suggestions that have been made over the years to model geniculate spontaneous activity have used either basic GRPs (Munemori et al., 1984), superpositions of GRPs, or random deletions of events from a GRP (Bishop et al., 1964). Later, more sophisticated methods have been developed with a view to incorporating the hidden temporal structure into the simulated spike trains, but they were still elaborations on the GRP: Levine and Troy (1986) proposed to modulate the rate of a GRP with Gaussian white noise, and Teich et al. (1997) found that a doubly stochastic GRP with fractal fluctuations in the rate could account for both the short- and long-term behavior (about 1 hr) of geniculate spontaneous firing.

Since the goal of our model was to simulate spontaneous and visually evoked geniculate spike trains on the order of 1 s, we considered that keeping the GRP as the core mechanism would be appropriate, given that long-term correlations are negligible over this time scale. The following sections explain why spontaneous activity, phasic responses, and tonic responses have been modelled with different regularity parameters r and how the values of r have been chosen.

Spontaneous discharge

We have chosen 10 spikes/s as a reasonable mean spontaneous firing rate. Bishop et al. (1964) have shown that cells with such activity levels are most often associated with under-dispersed gamma-like or exponential-like (their Figs. 3A–3B), long-interval histograms, and so-called type 1 short-interval histograms (their Fig. 5). The narrow peak near zero in long-interval histograms appears to be made of ISIs around 1–4 ms, which probably reflect the contribution of high- and low-threshold bursts, according to the criterion of Lo et al. (1991) (see short-interval histograms). If we neglect the occurrence of bursts during spontaneous activity, this allows us to smooth out the peak near zero in these histograms and to consider the ISI distribution as an under-dispersed gamma ($r > 1$) or an exponential ($r = 1$).

Also, Teich et al. (1997, Fig. 3B) show a typical geniculate ISI histogram that decreases linearly (in semilogarithmic scale) for interval durations greater than 50 ms, that is, for frequencies lower than 20 spikes/s. This means that the empirically estimated interval *pdf* is exponential (in linear scale) in a range containing the level of spontaneous activity we chose. This is consistent, to some extent, with spontaneous activity following a Poisson process. Additional support that spontaneous firing is almost Poisson in the anesthetized cat comes from Wilson et al. (1988, Fig. 1B). These authors showed that the ISI standard deviation and the mean ISI duration are linearly correlated with a slope close to one, which implies $r \approx 1$, by eqn. (5).

Visually evoked discharge

Identifying the kind of process that governs the visually evoked discharge is a difficult problem since responses are highly nonstationary. Most studies have addressed the issue of intertrial variability either in terms of mean rate or in terms of ISIs. Hartveit and Heggelund (1994) have shown that the variance of the mean firing rate increases linearly with the mean rate, in response to a spot flashed at different contrasts in the RF center. Levine et al. (1996) have reached the same conclusion for geniculate X-cells (Levine et al., 1996). Such a linear relationship is indeed what renewal theory predicts [eqn. (7)]. These experimental results support the assumption that visually evoked discharges follow a GRP.

What should be the value of r for the segment of the switching GRP associated with the visually evoked discharge? Wilson et al. (1988) provide evidence that visual responses to an optimal centered spot flashed in the RF center follow a GRP with $r > 1$, since the ISI standard deviation σ_T is linearly related to the mean interval μ_T with a slope slightly below 1 [eqn. (5)]. In contrast, Hartveit and Heggelund (1994) find that the variance of the estimated firing rate calculated from 500-ms samples increases linearly with the

mean rate with a proportionality factor $\nu = 4.51 \pm 2.13$. This combined with eqn. (7) yields an over-dispersed firing ($r = 0.44$). The evidence for $r > 1$ derived from Wilson et al. (1988) was preferred over the result of Hartveit and Heggelund (1994) because eqn. (5) relates μ_T and σ_T to r in an exact and straightforward manner, whereas inferring r from the estimated firing rate N_t/t makes it necessary to use eqn. (7), which is only an *approximation*.

We used an under-dispersed GRP ($r = 5$) to model phasic visual responses for the following additional reasons: first, Hartveit and Heggelund (1994) mentioned that, for several cells, the variance of the firing rate decreases at high discharge rates, which is consistent with a higher regularity for phasic responses than during spontaneous activity. Second, at high frequency as in the phasic response, the cell refractory period (about 1 ms) is no longer negligible with respect to the ISI. Using an over-dispersed gamma or exponential *pdf* would introduce very high frequency bursts, whereas an under-dispersed gamma *pdf* is a convenient way to incorporate a pseudorefractory period. Third, at firing frequencies around 65 spikes/s and above, the ISI is comparable to the mean duration of the retino-geniculate EPSP (10–40 ms, Coenen & Vendrik, 1972), so the low-pass filtering effect of the cell membrane would tend to smooth out the jitter in the retinal input and make the membrane potential variations more regular.

In the model, the strongest tonic discharge that can be obtained (when contrast $I = \pm 1$) is 60 spikes/s, with an optimal spot, since other stimuli would involve more CSA or less spatial summation in the center or both. The choice of 65 spikes/s as the switching frequency between high ($r = 5$) and low ($r = 1$) regularities guarantees that the more regular firing applies only to the phasic response. Given the lack of quantitative data, modelling tonic visual responses with simple Poisson processes was preferred.

Bursts versus single spikes

Unlike retinal ganglion cells, geniculate relay cells have a firing pattern that can vary between two extremes, tonic and burst (e.g. Sherman, 1996). Both modes have been shown to participate in geniculate receptive fields (Guido et al., 1992; Guido & Weyand, 1995). Bursts can have important synaptic effects and can convey significant visual information (Lisman, 1997; Reinagel et al., 1997). Up to recently (Guido et al., 1992; Mukherjee & Kaplan, 1995), the differential contribution of burst and tonic modes to geniculate visual responses had not been stressed. To identify the intrinsic channel properties responsible for the bursting activity patterns, Mukherjee and Kaplan (1995) combined computational modelling and simultaneous *in vivo* recordings of the retinal input and spike output of geniculate cells, and they stressed the critical role of the T-type calcium current. Burst firing has been shown to make a strong contribution to the initial phasic part of visual responses to gratings (Guido et al., 1992) and flashed spots (Guido & Sherman, 1998). Purely statistical analysis has shown that the initial phasic response, which contains a mixing of bursts and single spikes, has a higher regularity on average than either spontaneous activity or tonic response (Wilson et al., 1988). Hence, the increased regularity of geniculate firing during phasic response might directly reflect the increased contribution of bursts. In contrast to Mukherjee and Kaplan (1995), we do not model intrinsic channel properties explicitly, but their statistical contribution to the geniculate firing is indeed taken into account phenomenologically since phasic responses are generated with a high-regularity GRP. The influence of geniculate response regularity in the early decision process of a network of cortical simple cells is the subject of a forthcoming article.

Acknowledgments

We are grateful to Professor Murray Sherman and Dr. Jean Bullier for helpful suggestions to improve the manuscript and to Dr. Lionel Gabet for pointing to renewal theory at an early stage of this work. We thank Dr. Vincent Bringuier, Frédéric Chavane, and Valérie Ego for careful reading and criticisms and Nancy Rouillon for encouragement. Financial support to N. Gazères from the Ministry of Education and Research and the Association des Centraliens is gratefully acknowledged. This work is supported by grants from CNRS and GIS Cognisciences to Y. Frégnac.

References

Alonso, J.M., Usrey, W.M. & Reid, R.C. (1996). Precisely correlated firing in cells of the lateral geniculate nucleus. *Nature* **383**, 815–819.

Bishop, P.O., Levick, W.R. & Williams, W.O. (1964). Statistical analysis of the dark discharge of lateral geniculate neurones. *Journal of Physiology* (London) **170**, 598–612.

Borg-Graham, L.J. (1997). The Surf-Hippo Neuron Simulation System, version 2.7, http://www.cnrs-gif.fr/iaf/iaf9/surf-hippo.html.

Bullier, J. & Norton, T.T. (1979). X and Y relay cells in cat lateral geniculate nucleus: Quantitative analysis of receptive-field properties and classification. *Journal of Neurophysiology* **42**, 244–273.

Cleland, B.G., Dubin, M.W. & Levick, W.R. (1971). Simultaneous recording of input and output of lateral geniculate neurones. *Nature New Biology* **231**, 191–192.

Cleland, B.G. & Lee, B.B. (1985). A comparison of visual responses of cat lateral geniculate nucleus neurones with those of ganglion cells afferent to them. *Journal of Physiology* (London) **369**, 249–268.

Coenen, A.M.L. & Vendrik, A.J.H. (1972). Determination of the transfer ratio of cat's geniculate neurones through quasi-intracellular recordings and the relation with the level of alertness. *Experimental Brain Research* **14**, 227–242.

Cox, D.R. (1962). *Renewal Theory*. London: Methuen.

Enroth-Cugell, C. & Robson, J.G. (1966). The contrast sensitivity of retinal ganglion cells of the cat. *Journal of Physiology* (London) **187**, 517–552.

Fjeld, I.T., Ruksenas, O., Einevoll, G.T. & Heggelund, P. (1997). Spatial receptive field organization of dLGN neurons in cat. *Society for Neuroscience Abstracts* **23**, 73.4.

Gazères, N., Borg-Graham, L.J. & Frégnac, Y. (1997). A model of the ON/OFF organization of layer IV simple receptive fields in cat area 17. *Society for Neuroscience Abstracts* **23**, 801.15.

Guido, W., Lu, S.M. & Sherman, S.M. (1992). Relative contributions of burst and tonic responses to the receptive field properties of lateral geniculate neurones in the cat. *Journal of Neurophysiology* **68**, 2199–2211.

Guido, W. & Sherman, S.M. (1998). Response latencies of cells in the cat's lateral geniculate neurones are less variable during burst than tonic firing. *Visual Neuroscience* **15**, 231–237.

Guido, W. & Weyand, T. (1995). Burst responses in thalamic relay cells of the awake behaving cat. *Journal of Neurophysiology* **74**, 1782–1786.

Hamamoto, J., Cheng, H., Yoshida, K., Smith, E.L. & Chino, Y.M. (1994). Transfer characteristics of lateral geniculate nucleus X-neurons in the cat: Effects of temporal frequency. *Experimental Brain Research* **98**, 191–199.

Hammond, P. (1972). Chromatic sensitivity and spatial organization of LGN neurone receptive field in cat: Cone-rod interaction. *Journal of Physiology* (London) **225**, 391–413.

Hammond, P. (1973). Contrast in spatial organization of receptive fields at geniculate and retinal levels: Centre, surround and outer surround. *Journal of Physiology* (London) **228**, 115–137.

Hammond, P. & James, C.R. (1971). The Purkinje shift in cat: Extent of the mesopic range. *Journal of Physiology* (London) **216**, 99–109.

Hamos, J.E., Van Horn, S.C., Raczkowski, D. & Sherman, S.M. (1987). Synaptic circuits involving an individual retinogeniculate axon in the cat. *Journal of Comparative Neurology* **259**, 165–192.

Hartveit, E. & Heggelund, P. (1992). The effect of contrast on the visual response of lagged and non-lagged cells in the cat lateral geniculate nucleus. *Visual Neuroscience* **9**, 515–525.

Hartveit, E. & Heggelund, P. (1994). Response variability of single cells in the dorsal lateral geniculate nucleus of the cat. Comparison with retinal input and effect of brain stem stimulation. *Journal of Neurophysiology* **72**, 1278–1289.

HARTVEIT, E. & HEGGELUND, P. (1995). Brainstem modulation of signal transmission through the cat dorsal lateral geniculate nucleus. *Experimental Brain Research* **103**, 372–384.

HOFFMANN, K.P., STONE, J. & SHERMAN, S.M. (1972). Relay of receptive-field properties in the dorsal lateral geniculate nucleus of the cat. *Journal of Neurophysiology* **35**, 518–531.

HORTON, J.C. & SHERK, H. (1984). Receptive field properties in the cat's lateral geniculate nucleus in the absence of ON-center retinal input. *Journal of Neuroscience* **4**, 374–380.

HUBEL, D.H. & WIESEL, T.N. (1961). Integrative action in the cat's lateral geniculate body. *Journal of Physiology* (London) **155**, 385–398.

HUMPHREY, A.L. & WELLER, R.E. (1988). Functionally distinct groups of X-cells in the lateral geniculate nucleus of the cat. *Journal of Comparative Neurology* **268**, 429–447.

KAPLAN, E., MARCUS, S. & SO, Y.T. (1979). Effect of dark adaptation on spatial and temporal properties of receptive fields in cat lateral geniculate nucleus. *Journal of Physiology* (London) **294**, 561–580.

KAPLAN, E. & SHAPLEY, R. (1984). The origin of the S (slow) potential in the mammalian lateral geniculate nucleus. *Experimental Brain Research* **55**, 111–116.

KRATZ, K.E., WEBB, S.V. & SHERMAN, S.M. (1978). Electrophysiological classification of X- and Y-cells in the cat's lateral geniculate nucleus. *Vision Research* **18**, 1261–1264.

KUFFLER, S.W., FITZHUGH, R. & BARLOW, H.B. (1957). Maintained activity in the cat's retina in light and darkness. *Journal of General Physiology* **40**, 683–702.

LEVICK, W.R. & WILLIAMS, W.O. (1964). Maintained activity in lateral geniculate units in darkness. *Journal of Physiology* (London) **170**, 582–597.

LEVINE, M.W., CLELAND, B.G., MUKHERJEE, P. & KAPLAN, E. (1996). Tailoring of variability in the lateral geniculate nucleus of the cat. *Biological Cybernetics* **75**, 219–227.

LEVINE, M.W. & TROY, J.B. (1986). The variability of the maintained discharge of cat dorsal lateral geniculate cells. *Journal of Physiology* (London) **375**, 339–359.

LINSENMEIER, R.A., FRISHMAN, L.J., JAKIELA, H.G. & ENROTH-CUGELL, C. (1982). Receptive field properties of X and Y cells in the cat retina derived from contrast sensitivity measurements. *Vision Research* **22**, 1173–1183.

LISMAN, J.E. (1997). Bursts as a unit of neural information: Making unreliable synapses reliable. *Trends in Neuroscience* **20**, 38–43.

LIVINGSTONE, M.S. & HUBEL, D.H. (1981). Effect of sleep and arousal on the processing of visual information in the cat. *Nature* **291**, 554–561.

LO, F.S., LU, S.M. & SHERMAN, S.M. (1991). Intracellular and extracellular *in vivo* recording of different response modes for relay cells of the cat's lateral geniculate nucleus. *Experimental Brain Research* **83**, 317–328.

MAEX, R. & ORBAN, G.A. (1996). Model circuit of spiking neurones generating directional selectivity in simple cells. *Journal of Neurophysiology* **75**, 1515–1545.

MAFFEI, L. & FIORENTINI, A. (1972). Retinogeniculate convergence and analysis of contrast. *Journal of Neurophysiology* **35**, 65–72.

MASTRONARDE, D. (1983). Correlated firing of cat retinal ganglion cells. I. Spontaneously active inputs to X- and Y-cells. *Journal of Neurophysiology* **49**, 303–324.

MASTRONARDE, D. (1992). Nonlagged relay cells and interneurones in the cat lateral geniculate nucleus: Receptive-field properties and retinal inputs. *Visual Neuroscience* **8**, 407–441.

MUKHERJEE, P. & KAPLAN, E. (1995). Dynamics of neurons in the cat lateral geniculate nucleus: *In vivo* electrophysiology and computational modeling. *Journal of Neurophysiology* **74**, 1222–1243.

MUNEMORI, J., HARA, K., KIMURA, M. & SATO, R. (1984). Statistical features of impulse trains in cat's lateral geniculate neurones. *Biological Cybernetics* **50**, 167–172.

REINAGEL, P., GODWIN, D.W., SHERMAN, S.M., KOCH, C. (1997). Efficient information coding by LGN bursts. *Society for Neuroscience Abstracts* **23**, 73.7.

RICHTER, J. & ULLMAN, S. (1982). A model for the temporal organization of X- and Y-type receptive fields in the primate retina. *Biological Cybernetics* **43**, 127–145.

ROBSON, J.A. (1993). Qualitative and quantitative analyses of the patterns of retinal input to neurones in the dorsal lateral geniculate nucleus of the cat. *Journal of Comparative Neurology* **334**, 324–336.

RODIECK, R.W. (1965). Quantitative analysis of cat retinal ganglion cell responses to visual stimuli. *Vision Research* **5**, 583–601.

SAKAKURA, H. (1968). Spontaneous and evoked unitary activities of cat lateral geniculate neurones in sleep and wakefulness. *Japanese Journal of Physiology* **18**, 23–42.

SANDERSON, K.J. (1971). Visual field projection columns and magnification factors in the lateral geniculate nucleus of the cat. *Experimental Brain Research* **13**, 159–177.

SAUL, A.B. & HUMPHREY, A.L. (1990). Spatial and temporal response properties of lagged and nonlagged cells in cat lateral geniculate nucleus. *Journal of Neurophysiology* **64**, 206–224.

SESTOKAS, A.K., LEHMKÜHLE, S. & KRATZ, K.E. (1991). Relationship between response latency and amplitude for ganglion and geniculate X- and Y-cells in the cat. *International Journal of Neuroscience* **60**, 59–64.

SHERMAN, S.M. (1996). Dual response modes in lateral geniculate nucleus: Mechanisms and function. *Visual Neuroscience* **13**, 205–213.

SILLITO, A.M. & KEMP, J.A. (1983). The influence of GABAergic inhibitory processes on the receptive field structure of X and Y cells in cat dorsal lateral geniculate nucleus (dLGN). *Brain Research* **277**, 63–77.

SINGER, W. & CREUTZFELDT, O. (1972). Reciprocal lateral inhibition of ON- and OFF-center neurones in the lateral geniculate body of the cat. *Experimental Brain Research* **10**, 311–330.

SINGER, W., PÖPPEL, E. & CREUTZFELDT, O. (1970). Inhibitory interaction in the cat's lateral geniculate nucleus. *Experimental Brain Research* **14**, 210–226.

SO, Y.T. & SHAPLEY, R. (1979). Spatial properties of X and Y cells in the lateral geniculate nucleus of the cat and conduction velocities of their inputs. *Experimental Brain Research* **36**, 533–550.

SOMERS, D.C., NELSON, S.B. & SUR, M. (1995). An emergent model of orientation selectivity in cat visual cortical simple cells. *Journal of Neuroscience* **15**, 5448–5465.

TANAKA, K. (1983). Cross-correlation analysis of geniculostriate neuronal relationships in cats. *Journal of Neurophysiology* **49**, 1303–1318.

TEICH, M.C., HENEGHAN, C., LOWEN, S.B., OZAKI, T. & KAPLAN, E. (1997). Fractal character of the neural spike train in the visual system of the cat. *Journal of the Optical Society of America* **14**, 529–546.

VIDYASAGAR, T.R. & URBAS, J.V. (1982). Orientation selectivity of cat LGN neurones with and without visual inputs from visual cortical areas 17 and 18. *Experimental Brain Research* **46**, 157–169.

VIRSU, V., LEE, B.B. & CREUTZFELDT, O.D. (1977). Dark adaptation and receptive field organization in the cat lateral geniculate nucleus. *Experimental Brain Research* **27**, 35–50.

WEHMEIER, U., DONG, D., KOCH, C. & VAN ESSEN, D. (1989). Modelling the mammalian visual system. In *Methods in Neuronal Modelling*, ed. KOCH, C. & SEGEV, I., pp. 335–359. Cambridge, Massachusetts: MIT Press.

WILSON, J.R., BULLIER, J. & NORTON, T.T. (1988). Signal comparisons for X- and Y-cells in the retina and lateral geniculate nucleus of the cat. *Experimental Brain Research* **70**, 399–405.

WILSON, P.D., ROWE, M.H. & STONE, J. (1976). Properties of relay cells in cat's lateral geniculate nucleus: A comparison of W-cells with X- and Y-cells. *Journal of Neurophysiology* **39**, 1193–1209.

WÖRGÖTTER, F. & KOCH, C. (1991). A detailed model of the primary visual pathway in the cat: Comparison of afferent excitatory and intracortical inhibitory connection schemes for orientation selectivity. *Journal of Neuroscience* **11**, 1959–1979.

Appendix: Spatial integration of stationary bars and spots

The product of the stimulus R and the spatial filter G is defined by

$$p_0 = \langle G, R \rangle = \iint G(x,y)R(x,y)\,\mathrm{d}x\,\mathrm{d}y. \tag{A1}$$

When the stimulus $R(x,y)$ is the rectangular stationary bar shown in Fig. 1A, with its axes parallel to the axes of coordinates ($\theta = 0$)

$$p_0 = \int_{x_0-a/2}^{x_0+a/2} \frac{1}{\sqrt{2\pi}\sigma} \exp\left(-\frac{x^2}{2\sigma^2}\right) \mathrm{d}x$$

$$\times \int_{y_0-b/2}^{y_0+b/2} \frac{1}{\sqrt{2\pi}\sigma} \exp\left(-\frac{y^2}{2\sigma^2}\right) \mathrm{d}y.$$

Using the *error function* $erf(x) = (2/\sqrt{\pi})\int_0^x \exp(-t^2)\,dt$ leads to

$$p_0 = \frac{1}{4}\left[erf\left(\frac{x_0 + a/2}{\sigma\sqrt{2}}\right) - erf\left(\frac{x_0 - a/2}{\sigma\sqrt{2}}\right)\right] \times \left[erf\left(\frac{y_0 + b/2}{\sigma\sqrt{2}}\right) - erf\left(\frac{y_0 - b/2}{\sigma\sqrt{2}}\right)\right]. \quad \text{(A2)}$$

When the bar is tilted by θ deg with respect to the abscissa ($\theta \neq 0$), the integral of eqn. (A1) is left unchanged as the coordinate system is rotated by θ deg to bring its axes parallel to the axes of the bar, since the Gaussian is circular. Eqn. (A2) can then be used with a new center

$$x'_0 = x_0 \cos\theta + y_0 \sin\theta,$$

$$y'_0 = -x_0 \sin\theta + y_0 \cos\theta.$$

When the stimulus is a centered spot of diameter D, the output of the spatial filter is

$$p_0 = 1 - \exp(-D^2/8\sigma^2).$$

With stimulus contrast $I(t)$ defined as in eqn. (1), the *time-dependent* product of the stimulus and the Gaussian becomes

$$p(t) = p_0 I(t). \quad \text{(A3)}$$